

Scalable Bayesian inference for the generalized linear mixed model

Samuel I. Berchuck*, Felipe Medeiros, Sayan Mukherjee, Andrea Agazzi

March 6, 2024

Abstract

The generalized linear mixed model (GLMM) is a popular statistical approach for handling correlated data, and is used extensively in applications areas where big data is common, including biomedical data settings. The focus of this paper is scalable statistical inference for the GLMM, where we define statistical inference as: (i) estimation of population parameters, and (ii) evaluation of scientific hypotheses in the presence of uncertainty. Artificial intelligence (AI) learning algorithms excel at scalable statistical estimation, but rarely include uncertainty quantification. In contrast, Bayesian inference provides full statistical inference, since uncertainty quantification results automatically from the posterior distribution. Unfortunately, Bayesian inference algorithms, including Markov Chain Monte Carlo (MCMC), become computationally intractable in big data settings. In this paper, we introduce a statistical inference algorithm at the intersection of AI and Bayesian inference, that leverages the scalability of modern AI algorithms with guaranteed uncertainty quantification that accompanies Bayesian inference. Our algorithm is an extension of stochastic gradient MCMC with novel contributions that address the treatment of correlated data (i.e., intractable marginal likelihood) and proper posterior variance estimation. Through theoretical and empirical results we establish our algorithm's statistical inference properties, and apply the method in a large electronic health records database.

Keywords: Scalable statistical inference, stochastic gradient MCMC, Bayesian computational algorithms, uncertainty quantification, generalized linear mixed model

*Samuel I. Berchuck is an Assistant Professor, Department of Biostatistics & Bioinformatics, Statistical Science, Duke University, NC 27710 (E-mail: sib2@duke.edu). Felipe Medeiros is a Professor, Department of Ophthalmology, University of Miami, Miami, FL 33136 (E-mail: fmedeiros@med.miami.edu). Sayan Mukherjee is a Humboldt-Professor for Artificial Intelligence, Universität Leipzig, Leipzig, Germany, 04109 (E-mail: sayan.mukherjee@mis.mpg.de). Andrea Agazzi is an Assistant Professor, Department of Mathematics, Università di Pisa, Pisa, PI, Italy 56127 (E-mail: andrea.agazzi@unipi.it). Research reported in this publication was supported by the National Eye Institute of the National Institutes of Health (Bethesda, Maryland) under Awards Number R00EY033027 (SIB), R01EY029885 (FM), and R21EY031898 (FM). The sponsor or funding organization had no role in the design or conduct of this research. The content is solely the responsibility of the authors and does not necessarily represent the official views of the National Institutes of Health. AA is member of INdAM (GNAMPA group), and acknowledges partial support of Dipartimento di Eccellenza, UNIPI, the Future of Artificial Intelligence Research (FAIR) foundation (WP2), PRIN project ConStRAINeD, PRA Project APRiSE, and GNAMPA Project CUP_E53C22001930001.

1 Introduction

The generalized linear mixed model (GLMM) provides a framework for principally evaluating the association between predictors and an outcome in the presence of repeated measures; GLMMs are also widely used for prediction in this context (Agresti, 2012). For this reason, GLMMs have been extensively applied across settings where repeated measures are available, including biomedical data (Casals et al., 2014). In the digital era, where rapid data generation leads to big data, statistical inference for the GLMM becomes computationally intensive (Ormerod and Wand, 2012). Thus, developing scalable statistical inference algorithms is necessary to extend the usefulness of the GLMM into the big data era.

Statistical inference is concerned with drawing conclusions from a sample of data about unknown population quantities (i.e., parameters) that are not observed. To perform statistical inference requires both (i) estimation of population parameters, and (ii) evaluation of scientific hypotheses in the presence of uncertainty (Gelman et al., 1995). Uncertainty quantification is critical for hypothesis testing and communicating risk in prediction tasks and is often decomposed into aleatoric and epistemic (Der Kiureghian and Ditlevsen, 2009). Aleatoric uncertainty is regarded as irreducible and inherent to the data generating mechanism, while epistemic uncertainty results from incomplete knowledge and in principle can be reduced (Matthies, 2007). The decomposition of uncertainty and its role in statistical inference can be understood through the Bayesian posterior predictive distribution (PPD),

$$p(\mathbf{Y}_{i'} | \mathbf{Y}) = \int \underbrace{p(\mathbf{Y}_{i'} | \boldsymbol{\Omega})}_{\text{aleatoric}} \underbrace{p(\boldsymbol{\Omega} | \mathbf{Y})}_{\text{epistemic}} d\boldsymbol{\Omega},$$

for outcome vector $\mathbf{Y}_{i'}$ from new subject i' conditional on training data $\mathbf{Y} = (\mathbf{Y}_1^\top, \dots, \mathbf{Y}_n^\top)^\top$ and population parameters $\boldsymbol{\Omega} \in \mathbb{R}^d$. From this perspective, aleatoric uncertainty is rep-

resented through proper likelihood specification and epistemic uncertainty corresponds to uncertainty in parameter estimation, which in the Bayesian setting is entirely encoded in the posterior (Hüllermeier and Waegeman, 2021). In big data settings, reliable posterior estimation becomes difficult, leading to unreliable inference. In this paper, we focus on developing a scalable statistical inference algorithm that yields proper parameter estimation (i.e., epistemic uncertainty) and therefore reliable decision making.

In recent years, significant gains have been made in the development of scalable artificial intelligence (AI) algorithms for parameter estimation through stochastic optimization approaches, including stochastic gradient descent (SGD) and its variants (Robbins and Monro, 1951; Kingma and Ba, 2017). These algorithms facilitated the emergence of deep learning and led to countless scientific breakthroughs (Gulshan et al., 2016). While these algorithms enable scalable parameter estimation, uncertainty quantification is often ignored. Methods to quantify uncertainty in this setting have been introduced, including Monte Carlo dropout (Gal and Ghahramani, 2016), and ensemble learning (Abdar et al., 2021), however they are often computationally expensive. Bayesian inference, on the other hand, is considered a complete inference machine, since estimation and uncertainty are encoded by the posterior. Unfortunately, standard Bayesian inference algorithms, including Markov chain Monte Carlo (MCMC), are not inherently scalable (Miller and Dunson, 2019). In recent years, methods for improving efficiency of Bayesian inference have been introduced that leverage advances in AI algorithms, including stochastic gradient MCMC (SGMCMC).

SGMCMC is a class of algorithms derived from diffusion processes which admit the posterior as their invariant distribution (Nemeth and Fearnhead, 2021). The first variant of SGMCMC was introduced by Welling and Teh (2011), who described the stochastic gradient Langevin dynamics (SGLD) algorithm. While the properties of SGLD have been

studied with a decreasing step size (Teh et al., 2016), in practice constant step sizes are often used (Li et al., 2016). Often the step size is set to be proportional to the inverse of n , the number of samples, however this leads to an invariant distribution with an inflated variance (Brosse et al., 2018). Methods to alleviate this increased variance include preconditioning (Stephan et al., 2017), however in practice this approach is limited, since estimating the preconditioning matrix is computationally expensive (Vollmer et al., 2016). Other methods include stochastic gradient Hamiltonian Monte Carlo (Chen et al., 2014), Riemannian extensions (Patterson and Teh, 2013; Ma et al., 2015), and control variates to reduce the variance of the stochastic gradient (Baker et al., 2019). While these methods provide theoretical guarantees their practical impact has been limited due to computational limitations. In this paper, we focus our efforts on SGLD with an aim to make it a practical algorithm to be used for scalable statistical inference for the GLMM.

While an attractive algorithm for scalable inference, SGLD requires that the first order gradient of the log posterior distribution can be evaluated. Thus, extensions to dependent data settings are sparse, since the marginal log-likelihood is often not available in closed form. Existing extensions for dependent data include network data (Li et al., 2016), and hidden Markov models (Ma et al., 2017), however both of these applications leverage marginal likelihood specifications and are not generally applicable to other dependent data settings, including GLMM. Statistical inference for the GLMM requires frequent evaluation of the marginal likelihood, $p(\mathbf{Y}_i|\boldsymbol{\Omega}) = \int p(\mathbf{Y}_i|\boldsymbol{\gamma}_i, \boldsymbol{\Omega})p(\boldsymbol{\gamma}_i|\boldsymbol{\Omega})d\boldsymbol{\gamma}_i$, where $\boldsymbol{\gamma}_i \in \mathbb{R}^q$ is a vector of subject-specific parameters. In general, this q -dimensional integral does not have a closed-form, meaning SGLD can not be used in the GLMM setting without innovation.

In this paper, we introduce a scalable statistical inference algorithm for GLMM using a novel implementation of SGLD. The major contributions of the paper are as follows, (i)

we introduce a Monte Carlo estimator for the gradient of the marginal log-likelihood, thus permitting SGLD to be applied in the GLMM setting, (ii) we characterize the structure of the noise injected into the SGLD update and derive an asymptotic correction for the resulting biased estimate of the posterior covariance, in the large dataset regime, and (iii) we present empirical and real world results that demonstrate that our algorithm is a practical implementation of SGMC that can be used for proper inference in the GLMM setting.

2 Background and notation

We consider a database $\mathbf{Y} = (Y_1, \dots, Y_n)$ of size $n \in \mathbb{N}$, where Y_i represents the i -th observation for $i \in [n] := \{1, 2, \dots, n\}$. For population parameter $\boldsymbol{\Omega} \in \mathbb{R}^d$ we aim to estimate the posterior distribution, $\pi(\boldsymbol{\Omega}) := p(\boldsymbol{\Omega}|\mathbf{Y}) \propto p(\boldsymbol{\Omega}) \prod_{i=1}^n p(Y_i|\boldsymbol{\Omega})$, where $p(\boldsymbol{\Omega})$ is a prior distribution for the parameters $\boldsymbol{\Omega}$, $p(Y_i|\boldsymbol{\Omega})$ is the likelihood function and \propto denotes proportionality up to a constant. For notational convenience, we define $f_i(\boldsymbol{\Omega}) = -\log p(Y_i|\boldsymbol{\Omega})$ for all i , where $f_0(\boldsymbol{\Omega}) = -\log p(\boldsymbol{\Omega})$ and $f(\boldsymbol{\Omega}) = \sum_{i=0}^n f_i(\boldsymbol{\Omega})$. The posterior density can then be rewritten as, $\pi(\boldsymbol{\Omega}) \propto \exp\{-f(\boldsymbol{\Omega})\}$.

2.1 Stochastic gradient Langevin dynamics

The Langevin diffusion, $\boldsymbol{\Omega}_t$, is defined by the stochastic differential equation (SDE),

$$d\boldsymbol{\Omega}_t = -\nabla f(\boldsymbol{\Omega}_t) dt + \sqrt{2}d\mathbf{B}_t, \quad (1)$$

where $\nabla f(\boldsymbol{\Omega})$ denotes the gradient of f in $\boldsymbol{\Omega}$ and \mathbf{B}_t is a d -dimensional Brownian motion. Under mild regularity conditions on f , the stationary distribution of this diffusion is the posterior, so that samples from π can theoretically be obtained from stationary trajectories

of (1). In practice, to sample from (1) we must discretize it. The Langevin diffusion solving (1) can be approximated using the Euler-Mauryama discretization with step-size $\epsilon > 0$,

$$\boldsymbol{\Omega}_{k+1} = \boldsymbol{\Omega}_k - \epsilon \nabla f(\boldsymbol{\Omega}_k) + \sqrt{2\epsilon} \boldsymbol{\eta}_k, \quad \boldsymbol{\eta}_k \stackrel{iid}{\sim} \mathcal{N}_d(\mathbf{0}, \mathbf{I}_d). \quad (2)$$

Since $\nabla f(\boldsymbol{\Omega}) = \nabla f_0(\boldsymbol{\Omega}) + \sum_{i=1}^n \nabla f_i(\boldsymbol{\Omega})$, the update of (2) has a computational cost that scales linearly in n . In the regime $n \gg 1$ (i.e., the big data regime of interest for this paper), this results in a prohibitive computational cost for the sampling process. In response to this observation, Welling and Teh (2011) introduced SGLD by replacing the full-data gradient $\nabla f(\boldsymbol{\Omega})$ with an unbiased estimate $\hat{\nabla f}(\boldsymbol{\Omega}) = \nabla f_0(\boldsymbol{\Omega}) + \frac{n}{S} \sum_{i \in \mathcal{S}} \nabla f_i(\boldsymbol{\Omega})$, where \mathcal{S} is a subset of $[n]$ with $|\mathcal{S}| = S$. When $S \ll n$, this significantly reduces the cost of the gradient computation. A single update of the vanilla SGLD algorithm is thus given by,

$$\boldsymbol{\Omega}_{k+1} = \boldsymbol{\Omega}_k - \epsilon \hat{\nabla f}(\boldsymbol{\Omega}_k) + \kappa \sqrt{2\epsilon} \boldsymbol{\eta}_k, \quad (3)$$

where $\kappa = 1$ and we recall that $\epsilon > 0$ corresponds to a fixed step-size. The case $\kappa = 0$, where the minibatch randomness is the only source of noise, corresponds to SGD. SGLD (and simpler variant SGD) has been routinely applied in independent data settings, however applications in the dependent setting are limited due to computational complexities in approximating the marginal log-likelihood. In the next section, we introduce GLMM notation and detail how SGLD must be adapted in order to be used in the GLMM setting.

2.2 Generalized linear mixed model

In GLMM, each subject $i \in [n]$ has $n_i \in \mathbb{N}$ repeated measures, Y_{it} for $t \in [n_i]$. Let \mathbf{x}_{it} denote a p -dimensional vector of covariates, and \mathbf{z}_{it} denote a q -dimensional vector of covariates

that are assumed to have subject-specific parameters. The elements of $\mathbf{Y}_i = (Y_{i1}, \dots, Y_{in_i})^\top$ are modeled as conditionally independent random variables from the exponential family,

$$p(Y_{it}|\theta_{it}, \phi) = \exp \left\{ \frac{Y_{it}\theta_{it} - b(\theta_{it})}{a(\phi)} + c(Y_{it}, \phi) \right\},$$

where θ_{it} is a canonical parameter related to the linear predictor $\eta_{it} = \mathbf{x}_{it}^\top \boldsymbol{\beta} + \mathbf{z}_{it}^\top \boldsymbol{\gamma}_i$. The parameter $\boldsymbol{\beta}$ is a p -dimensional vector of population regression parameters (sometimes referred to as fixed effects) and $\boldsymbol{\gamma}_i$ is a q -dimensional vector of subject-specific parameter deviations from the population parameters (sometimes referred to as random effects). The subject-specific parameters are assumed to have the following distribution, $\boldsymbol{\gamma}_i \stackrel{\text{iid}}{\sim} \mathcal{N}_q(0, \boldsymbol{\Sigma})$, although our method generalizes naturally outside this setting. The parameter ϕ is an m -dimensional dispersion vector and $a(\cdot), b(\cdot), c(\cdot)$ are known functions that output a scalar. The canonical link function, $d(\cdot)$, is obtained when $\theta_{it} = \eta_{it}$ which is when $d(\mu_{it}) = \theta_{it}$, where $\mu_{it} = \mathbb{E}[Y_{it}|\boldsymbol{\beta}, \boldsymbol{\gamma}_i, \phi]$. Population parameters are grouped as $\boldsymbol{\Omega} = (\boldsymbol{\beta}, \boldsymbol{\Sigma}, \phi)$.

We are interested in the the posterior distribution, $p(\boldsymbol{\Omega}|\mathbf{Y})$, where $\mathbf{Y} = (\mathbf{Y}_1^\top, \dots, \mathbf{Y}_n^\top)^\top$. The posterior is proportional to the marginal joint likelihood times the prior, $\pi(\boldsymbol{\Omega}) := p(\boldsymbol{\Omega}|\mathbf{Y}) \propto p(\mathbf{Y}|\boldsymbol{\Omega})p(\boldsymbol{\Omega})$, where we assume that the prior and likelihood decompose as $p(\boldsymbol{\Omega}) = p(\boldsymbol{\beta})p(\boldsymbol{\Sigma})p(\phi)$ and $p(\mathbf{Y}|\boldsymbol{\Omega}) = \prod_{i=1}^n p(\mathbf{Y}_i|\boldsymbol{\Omega})$. The subject-specific likelihood contribution is given by the following q -dimensional integral that in general is intractable,

$$p(\mathbf{Y}_i|\boldsymbol{\Omega}) = \int \prod_{t=1}^{n_i} p(Y_{it}|\boldsymbol{\beta}, \boldsymbol{\gamma}_i, \phi) p(\boldsymbol{\gamma}_i|\boldsymbol{\Sigma}) d\boldsymbol{\gamma}_i. \quad (4)$$

In rare exceptions, including the Gaussian case, the integral may have a closed-form, however tractability typically breaks down when the subject-specific parameters have a distribution that is non-Gaussian. Thus, to perform inference in this setting requires approximating

(4). In the next section, we describe existing techniques for overcoming this integral.

2.3 Methods of inference for the GLMM

There are numerous approaches for performing inference in the GLMM setting, including likelihood-based, Monte Carlo, and Bayesian inference. Likelihood-based approaches, including Laplace approximation (Tierney et al., 1989), adaptive Gaussian-Hermite quadrature (Naylor and Smith, 1982), and penalized quasi-likelihood (Breslow and Clayton, 1993), don't generalize well when q is large and the random effects distribution is non-Gaussian. Monte Carlo methods are more flexible, and, among others, include bridge sampling (Frühwirth-Schnatter, 2004), and Chib's method (Chib, 1995; Chib and Jeliazkov, 2001). While highly flexible, each of these methods have issues, including large variances and difficult to define proposal distributions. Monte Carlo methods have also been used in concert with the expectation-maximization (EM) algorithm (Booth and Hobert, 1999), with corresponding stochastic approximations (Meza et al., 2009).

Bayesian inference for the GLMM uses the conditional likelihood and standard MCMC algorithms can be used, including Gibbs sampling (Gelman et al., 1995). However, in large samples this becomes computationally infeasible due to the growing size of the subject-specific parameters. To alleviate this computational burden, approximate Bayesian methods have been introduced, including integrated nested Laplace approximation (INLA) (Rue et al., 2017), and variational Bayesian inference (Tan and Nott, 2013; Ormerod and Wand, 2012). In large samples, Bayesian methods become computationally demanding due to the growing size of the subject-specific parameters. Marginal approaches alleviate this computational bottleneck, however, must contend with the integral in (4).

Motivated by gradient based estimation approaches, including SGMCMC, an alternative

approach has emerged that approximates the gradient of the marginal log-likelihood, and most often relies on Fisher’s identity (Fisher, 1925). Fisher’s identity aims to approximate $g_i(\Omega) = \nabla f_i(\Omega) = -\nabla \log p(\mathbf{Y}_i|\Omega)$, by writing it as an expectation with respect to the posterior distribution of the subject-specific parameters, $p(\gamma_i|\mathbf{Y}_i, \Omega)$,

$$g_i(\Omega) = \mathbb{E}_{\gamma_i|\mathbf{Y}_i, \Omega} [-\nabla \log p(\mathbf{Y}_i, \gamma_i|\Omega)]. \quad (5)$$

This approach has been used in settings with latent variables, including linear dynamic systems (Segal and Weinstein, 1989), non-linear and non-Gaussian state space models (Kantas et al., 2015), and inverse problems (Jasra et al., 2021), among others. Tran et al. (2020) used Fisher’s identity to incorporate neural networks into a variational Bayesian approach within the context of GLMM. Their method estimated the gradient of the conditional log-likelihood using back-propagation and then estimated the integral using importance sampling. In this approach, uncertainty is dependent on the Gaussian variational approximation and the uncertainty in estimating $g_i(\Omega)$ is ignored. In our paper, similar to Tran et al. (2020), we approach inference using Fisher’s identity to approximate the gradient of the marginal log-likelihood, thus permitting inference using SGMCMC algorithms.

3 Scalable Bayesian inference for GLMM

In this section, we introduce our algorithm for performing scalable Bayesian inference for GLMMs. We start by defining a Monte Carlo estimator for the gradient of the marginal log-likelihood and show how to use it within SGLD to get posterior samples with proper variance using a covariance correction. We provide both heuristic and theoretical justification for the covariance correction and present a practical guide for algorithmic implementation.

3.1 Overcoming the intractable marginal likelihood

Similar to Tran et al. (2020), we take a Monte Carlo approach to estimating $g_i(\Omega)$. We define our Monte Carlo estimator for the RHS of (5) as,

$$\hat{g}_i(\Omega) = -\frac{1}{R} \sum_{r=1}^R \nabla \log p(\mathbf{Y}_i, \gamma_{ir} | \Omega), \quad \gamma_{ir} \stackrel{iid}{\sim} p(\gamma_i | \mathbf{Y}_i, \Omega). \quad (6)$$

This estimator can be computed easily, since the gradient, $\nabla \log p(\mathbf{Y}_i, \gamma_{ir} | \Omega)$, is available analytically, and samples from the posterior $p(\gamma_i | \mathbf{Y}_i, \Omega)$ can be obtained from standard MCMC. We describe these calculations leading to (6) in more details in Section 3.4. Denoting by $\mathbb{V}_{\mathbf{X}|\mathbf{Y}}(f(\mathbf{X}))$ the conditional covariance of $f(\mathbf{X})$ given \mathbf{Y} we define,

$$\Psi_i(\Omega) = \mathbb{V}_{\gamma_i | \mathbf{Y}_i, \Omega}(\hat{g}_i(\Omega)) = \frac{1}{R} \mathbb{V}_{\gamma_i | \mathbf{Y}_i, \Omega}(\nabla \log p(\mathbf{Y}_i, \gamma_i | \Omega)). \quad (7)$$

as the covariance of the Monte Carlo estimator (6). This covariance can be estimated as,

$$\hat{\Psi}_i(\Omega) = \frac{1}{R(R-1)} \sum_{r=1}^R (\nabla \log p(\mathbf{Y}_i, \gamma_{ir} | \Omega) - \hat{g}_i(\Omega)) (\nabla \log p(\mathbf{Y}_i, \gamma_{ir} | \Omega) - \hat{g}_i(\Omega))^\top.$$

Lemma 3.1. *For all $i \in [n]$, $\hat{g}_i(\Omega)$ as defined in (6) and $\hat{\Psi}_i(\Omega)$ as defined in (7) are unbiased estimators of the gradient of the marginal log-likelihood, $g_i(\Omega)$, and the covariance matrix $\Psi_i(\Omega)$, respectively.*

Proof. The proof is given in Section A of the supplementary materials. \square

Having characterized the properties of (6) for an observation i , we proceed to study the statistical properties of the minibatch estimate of the *population* gradient. In doing so, we account for the uncertainty from (i) sampling a minibatch, and (ii) the Monte Carlo estimator as defined in Lemma 3.1. For a minibatch \mathcal{S} of size S , we define the \mathcal{S} -minibatch

gradient as, $\bar{g}_S(\Omega) = \frac{1}{S} \sum_{i \in S} \hat{g}_i(\Omega)$ and the true gradient as $\bar{g}_n(\Omega) = \frac{1}{n} \sum_{i=1}^n g_i(\Omega)$.

Lemma 3.2. *For every Ω , $\bar{g}_S(\Omega)$ is an unbiased estimator of $\bar{g}_n(\Omega)$ with covariance $S^{-1}\Psi(\Omega)$ and $\Psi(\Omega) = n^{-1} \sum_{i=1}^n (g_i(\Omega) - \bar{g}_n(\Omega)) (g_i(\Omega) - \bar{g}_n(\Omega))^T + \Psi_i(\Omega)$. Furthermore,*

$$\hat{\Psi}(\Omega) := \frac{1}{n} \sum_{i=1}^n (\hat{g}_i(\Omega) - \hat{\bar{g}}_n(\Omega)) (\hat{g}_i(\Omega) - \hat{\bar{g}}_n(\Omega))^T + \frac{\hat{\Psi}_i(\Omega)}{n},$$

is an unbiased estimator of $\Psi(\Omega)$, where $\hat{\bar{g}}_n(\Omega) = \frac{1}{n} \sum_{i=1}^n \hat{g}_i(\Omega)$.

Proof. The proof is given in Section B of the supplementary materials. \square

Using Lemma 3.2, we can rewrite the SGLD update to expose the added noise,

$$\begin{aligned} \Omega_{k+1} - \Omega_k &= -\epsilon \left(\nabla f_0(\Omega_k) + \frac{n}{S} \sum_{i \in S_k} \hat{g}_i(\Omega_k) \right) + \kappa \sqrt{2\epsilon} \boldsymbol{\eta}_k \\ &= -\epsilon \nabla f(\Omega) + \sqrt{2\epsilon} \left(\sqrt{\frac{\epsilon n^2}{2S}} \boldsymbol{\xi}_k + \kappa \boldsymbol{\eta}_k \right) \end{aligned} \quad (8)$$

where $\boldsymbol{\xi}_k$ is a set of *iid* random variables independent of $\boldsymbol{\eta}_k$ with covariance $\mathbb{V}(\boldsymbol{\xi}_k) = \Psi(\Omega_k)$.

3.2 Heuristics for a covariance correction

We now perform a heuristic computation that will drive the intuition behind the theoretical results presented in the following section. To study the asymptotic properties of the quantities of interest in the relevant regime $n \rightarrow \infty$, we introduce the notation $g = O_n(a_n)$, $g = \Omega_n(a_n)$ to mean that there exists $M > 0$ for which $\|g\| \leq Ma_n$, respectively $\|g\| \geq Ma_n$ as $n \rightarrow \infty$. We start by approximating the discrete-time update in (8) with a forward Euler-Mauryama update of matching mean and variance,

$$\Omega_{k+1} - \Omega_k = -\epsilon \nabla f(\Omega) + \sqrt{2\epsilon} \boldsymbol{\eta}'_k, \quad \boldsymbol{\eta}'_k \sim \mathcal{N}(\mathbf{0}, \Gamma(\Omega_k)),$$

where $\mathbf{\Gamma}(\mathbf{\Omega}) = \epsilon n^2 \mathbf{\Psi}(\mathbf{\Omega})/(2S) + \kappa \mathbf{I}_d$. The update approximates the evolution of the SDE, $d\mathbf{\Omega}_t = -\nabla f(\mathbf{\Omega}_t)dt + \sigma(\mathbf{\Omega}_t)d\mathbf{B}_t$ for $\sigma(\mathbf{\Omega})\sigma(\mathbf{\Omega})^\top = \mathbf{\Gamma}(\mathbf{\Omega})$. By the law of large numbers, we expect $n^{-1}\nabla f(\mathbf{\Omega})$ to converge to an n -independent function of $\mathbf{\Omega}$ so that $\nabla f(\mathbf{\Omega}) = \Omega_n(n)$ for $\mathbf{\Omega} \neq \mathbf{\Omega}^*$. Consequently, the distribution of $\mathbf{\Omega}_t$ will concentrate around the minimizer $\mathbf{\Omega}^*$ of f justifying the linearization of the SDE approximation of the update around $\mathbf{\Omega}^*$,

$$d(\mathbf{\Omega}_t - \mathbf{\Omega}^*) = -\nabla^2 f(\mathbf{\Omega}^*)(\mathbf{\Omega}_t - \mathbf{\Omega}^*)dt + \sigma(\mathbf{\Omega}^*)d\mathbf{B}_t.$$

The invariant measure of this linear equation can be explicitly computed as $\bar{\pi}(\mathbf{\Omega}) = Z^{-1} \exp \{ -(\mathbf{\Omega} - \mathbf{\Omega}^*)^\top \mathbf{\Sigma}^{-1}(\mathbf{\Omega} - \mathbf{\Omega}^*)/2 \}$, where $\mathbf{\Sigma}$ satisfies the Lyapunov equation,

$$\mathbf{A}\mathbf{\Sigma} + \mathbf{\Sigma}\mathbf{A}^\top = 2\mathbf{\Gamma}, \quad (9)$$

for $\mathbf{A} = \nabla^2 f(\mathbf{\Omega}^*)$ and $\mathbf{\Gamma} = \epsilon n^2 \mathbf{\Psi}(\mathbf{\Omega}^*)/(2S) + \kappa \mathbf{I}_d$. Since both $\mathbf{\Sigma}$ and \mathbf{A} are symmetric, (9) can be written as $\mathbf{\Sigma}\mathbf{A} + \mathbf{A}\mathbf{\Sigma} = 2\mathbf{\Gamma}$. Solving this equation for \mathbf{A} , where $\mathbf{\Sigma}, \mathbf{\Gamma}$ are estimated from SGLD samples, yields an accurate estimate of the desired covariance.

Remark 3.3. Note that, whenever $\epsilon/S = \Omega_n(n^{-2})$, the contribution $\kappa \mathbf{I}_d$ of the injected noise from the Langevin dynamics becomes negligible with respect to the one resulting from the minibatch stochastic approximation of the gradient. In this sense, analyzing SGD or SGLD ($\kappa = 0$ or $\kappa = 1$) results in the same leading order asymptotics.

3.3 Ergodic properties of $\mathbf{SG}(\mathbf{L})\mathbf{D}$

In this section, we recall some estimates from Brosse et al. (2018) proving geometric ergodicity of SGLD and extend some bounds on the associated ergodic (invariant) measure, from the same reference, to verify the intuition developed in the previous section. First,

we state some necessary assumptions,

Assumption 1. For all $j \in [n]$, f_j is convex, is four times continuously differentiable and there exists a constant $L > 0$ such that for all $\ell \in \{2, 3, 4\}$ it holds that $\sup_{\Omega} \|D^\ell f_j(\Omega)\| \leq L$. Furthermore, we assume that f is M -strongly convex (i.e., for any Ω, Ω' we have $\langle g(\Omega) - g(\Omega'), \Omega - \Omega' \rangle \geq M\|\Omega - \Omega'\|^2$).

L -Lipschitz continuous: for all Ω, Ω' we have $\|g_j(\Omega) - g_j(\Omega')\| \leq L\|\Omega - \Omega'\|$. The above assumption also implies that f has a unique minimizer, which will be denoted as Ω^* throughout. We report the following result from (Brosse et al., 2018, Lemma 1), adapting its notation. This result establishes existence and uniqueness of an invariant measure for the process Ω_k from (3) and geometric convergence of the distribution of Ω_k to such invariant measure. Here, we denote by $\mathcal{P}_2(\mathbb{R}^d)$ the space of probability measures on \mathbb{R}^d with finite second moments, by $W_2^2(\mu, \nu)$ the Wasserstein 2-distance between $\mu, \nu \in \mathcal{P}^2$ and by $P_k(\Omega_0, \cdot) = \mathbb{P}(\Omega_k \in \cdot)$ the distribution of Ω_k with initial condition Ω_0 .

Lemma 3.4. Under Assumption 1, for any step size $\epsilon \in (0, 2(Ln)^{-1})$, Ω_k defined as in (3) has a unique invariant measure $\tilde{\pi} \in \mathcal{P}_2(\mathbb{R}^d)$. In addition, for all $\epsilon \in (0, 1/(Ln)^{-1}]$, $\Omega_0 \in \mathbb{R}^d$ and $k \in \mathbb{N}$, we have that,

$$W_2^2(P_k(\Omega_0, \cdot), \tilde{\pi}) \leq (1 - M\epsilon)^k \int_{\mathbb{R}^d} \|\Omega_0 - \Omega\|^2 \tilde{\pi}(d\Omega).$$

Adapting a result from the same reference, we now proceed to estimate the mean and covariance, $\tilde{\Sigma} = \int_{\mathbb{R}^d} (\Omega - \Omega^*)^{\otimes 2} \tilde{\pi}(d\Omega)$, of such invariant distribution in the limit $n \rightarrow \infty$, relating it to the corresponding quantities for the distribution π , that we aim to estimate.

Theorem 3.5. Let Assumption 1 hold and recall the definition $\mathbf{A} := \nabla^2 f(\Omega^*)$. Set $\epsilon =$

$Sn^{-(1+\delta)}$ for a $\delta \in (0, 1]$ and assume that $\liminf_{n \rightarrow +\infty} nM^{-1} > 0$. Then,

$$\tilde{\Sigma} \mathbf{A} + \mathbf{A} \tilde{\Sigma} = 2\Gamma \left(1 + O_n(n^{-\min(1-\delta, \delta/2)}) \right).$$

Proof. The proof is given in Section C of the supplementary materials. \square

Finally, the following proposition clarifies the connection between the matrix $\mathbf{A} = \nabla^2 f(\Omega^*)$ and the covariance of π we aim to estimate. The proof is given in Brosse et al. (2018). Note that, under Assumption 1, both quantities scale like $O_n(n^{-1})$.

Proposition 3.6. *Let Assumption 1 hold and assume that $\liminf_{n \rightarrow \infty} n^{-1}M > 0$. Then,*

$$\int_{\mathbb{R}^d} (\Omega - \Omega^*)^{\otimes 2} \pi(d\Omega) = \nabla^2 f(\Omega^*)^{-1} + O_n(n^{-3/2}),$$

and,

$$\int_{\mathbb{R}^d} \Omega \pi(d\theta) - \Omega^* = -\frac{1}{2} \nabla^2 f(\Omega^*)^{-1} D^3 f(\Omega^*) [\nabla^2 f(\Omega^*)^{-1}] + O_n(n^{-3/2}).$$

3.4 Practical implementation of the algorithm

Using the heuristic and theoretical analysis given in the two preceding sections, we describe how to obtain posterior samples from our algorithm. We begin by solving the Lyapunov equation in (9), where \mathbf{A}^{-1} represents the true posterior covariance, Σ represents the incorrect covariance computed from the raw SGLD samples, and Γ represents injected noise in the SDE. We define the Cholesky decomposition for the uncorrected and corrected covariance as, $\Sigma = \mathbf{E}^\top \mathbf{E}$ and $\mathbf{A} = \mathbf{F}^\top \mathbf{F}$. The corrected samples can be computed as follows,

$$\Theta_k = \mathbf{G} (\Omega_k - \Omega^*) + \Omega^*, \quad \mathbf{G} = (\mathbf{E}^\top \mathbf{F})^{-1}. \quad (10)$$

Algorithm 1 SGLD with Covariance Correction

Require: $\Omega_0, S, \delta, K, R, \kappa$

Define $\epsilon = S/n^{1+\delta}$
for $k \in 1, \dots, K$ **do**

 Draw $\mathcal{S}_k \sim \mathcal{S}$

 for $i \in \mathcal{S}_k$ **do**

 Initialize: γ_{i0}

 for $r \in 1, \dots, R$ **do**

 Sample γ_{ir} from $p(\gamma_i | \mathbf{Y}_i, \Omega)$

 Compute $\nabla_{\Omega} \log p(\mathbf{Y}_i, \gamma_{ir} | \Omega)$

 end for

 Compute $\hat{g}_i(\Omega_k) = \frac{1}{R} \sum_{r=1}^R \nabla_{\Omega} \log p(\mathbf{Y}_i, \gamma_{ir} | \Omega)$

 end for

 Compute $\hat{g}_{\mathcal{S}_k}(\Omega_k) = \frac{1}{S} \sum_{i \in \mathcal{S}_k} \hat{g}_i(\Omega_k)$

 Draw $\eta_k \sim N(0, 2\epsilon \mathbf{I}_d)$

 $\Omega_{k+1} \leftarrow \Omega_k - \epsilon (\nabla f_0(\Omega_k) + n\bar{g}_{\mathcal{S}_k}(\Omega_k)) + \kappa \eta_k$
end for

Compute posterior mean of unconstrained parameters, Ω^*

Compute correction, $\hat{\Psi}(\Omega^*)$ ▷ Computation for $\hat{\Psi}(\Omega)$ is given in Lemma 3.2

Obtain corrected samples Θ_k ▷ Definition of Θ_k is given in (10)

The samples Θ_k will then have the proper mean and covariance (i.e., $\mathbb{V}(\Theta_k) = \mathbf{A}^{-1}$). In practice, Ω^* is the posterior mean. The algorithm is detailed in Algorithm 1.

To compute the Monte Carlo estimator, we must compute $\nabla \log p(\mathbf{Y}_i, \gamma_{ir} | \Omega)$. In general, these gradients can be computed using auto-differentiation, making our method highly generalizable, however in the GLMM setting the gradients are straightforward and are presented here. The gradient with respect to the population regression parameter β is,

$$\nabla_{\beta} \log p(\mathbf{Y}_i, \gamma_{ir} | \Omega) = \frac{\mathbf{X}_i^{\top} (\mathbf{Y}_i - \mu_{ir})}{a(\phi)}, \quad (11)$$

where $\mathbf{X}_i = (\mathbf{x}_{i1}, \dots, \mathbf{x}_{in_i})^{\top}$ is an $n_i \times p$ dimensional matrix of covariates and $\mu_{ir} = (\mu_{ir1}, \dots, \mu_{irn_i})^{\top}$ is an n_i -dimensional vector. The subject-specific parameters are introduced through the mean function, $\mu_{irt} = d^{-1}(\theta_{irt})$, where $\theta_{irt} = \mathbf{x}_{it}^{\top} \beta + \mathbf{z}_{it}^{\top} \gamma_{ir}$. Note that the gradient in (11) comes from properties of the log-cumulant function, $b(\theta_{irt})$, namely

that its derivatives yield moments of the distribution. The gradient with respect to the dispersion parameter can be computed as follows,

$$\nabla_{\phi} \log f(\mathbf{Y}_i, \boldsymbol{\gamma}_{ir} | \boldsymbol{\Omega}) = - \sum_{t=1}^{n_i} \left[\frac{Y_{it}\theta_{irt} - b(\theta_{irt})}{a'(\phi)a(\phi)^2} \right] + c'(Y_{it}, \phi), \quad (12)$$

where $a'(\phi)$ and $c'(Y_{it}, \phi)$ are derivatives with respect to ϕ . The gradient for $\boldsymbol{\Sigma}$ reduces to, $\nabla_{\boldsymbol{\Sigma}} \log f(\mathbf{Y}_i, \boldsymbol{\gamma}_{ir} | \boldsymbol{\Omega}) = \nabla_{\boldsymbol{\Sigma}} \log f(\boldsymbol{\gamma}_{ir} | \boldsymbol{\Sigma})$ and is highly dependent on the distributional assumptions of the subject-specific parameters. In (13), we compute these gradients for a particular specification, namely a bivariate Gaussian distribution.

4 Simulations

In this section, we demonstrate the performance of our algorithm in various GLMM settings. We show that our algorithm properly estimates the posterior mean and variance and is a viable technique when the sample size becomes large, in contrast to Gibbs sampling. We begin by establishing our algorithm in the linear mixed model setting (i.e., Gaussian distribution) with known variance components. We then study the setting where variance components must be estimated and under various distributional assumptions, including Gaussian, Bernoulli, and Poisson. We demonstrate that our algorithm allows for proper inference for GLMMs, even for large n where standard inference algorithms falter.

4.1 Gaussian with Fixed Variance Components

For our first simulation, we used a data generating mechanism where the posterior can be found in closed form. We assumed a linear mixed model, $\mathbf{Y}_i = \mathbf{X}_i\boldsymbol{\beta} + \mathbf{X}_i\boldsymbol{\gamma}_i + \boldsymbol{\epsilon}_i$, $\boldsymbol{\epsilon}_i \stackrel{iid}{\sim} \mathcal{N}(\mathbf{0}, \sigma^2 \mathbf{I}_{n_i})$ and $\boldsymbol{\gamma}_i | \boldsymbol{\Sigma} \stackrel{iid}{\sim} \mathcal{N}(\mathbf{0}, \boldsymbol{\Sigma})$ with $\boldsymbol{\Sigma}$ and σ^2 fixed. The marginal can be computed

analytically and is given by $\mathbf{Y}_i|\boldsymbol{\beta} \stackrel{ind}{\sim} \mathcal{N}(\mathbf{X}_i\boldsymbol{\beta}, \boldsymbol{\Upsilon}_i)$, where $\boldsymbol{\Upsilon}_i = \sigma^2 \mathbf{I}_{n_i} + \mathbf{X}_i \boldsymbol{\Sigma} \mathbf{X}_i^\top$. Since the likelihood is Gaussian, we can find the following three quantities in closed form,

1. **Posterior distribution for $\boldsymbol{\beta}$:** $\boldsymbol{\beta}|\mathbf{Y} \sim \mathcal{N}(\mathbf{A}^{-1}\mathbf{B}, \mathbf{A}^{-1})$, $\mathbf{A} = \sum_{i=1}^n \mathbf{X}_i^\top \boldsymbol{\Upsilon}_i^{-1} \mathbf{X}_i + \sigma_\beta^{-2} \mathbf{I}_p$ and $\mathbf{B} = \sum_{i=1}^n \mathbf{X}_i^\top \boldsymbol{\Upsilon}_i^{-1} \mathbf{Y}_i$, where $\mathbf{Y} = (\mathbf{Y}_1^\top, \dots, \mathbf{Y}_n^\top)^\top$.
2. **Gradient of the marginal log likelihood:** $\nabla_{\boldsymbol{\beta}} \log p(\mathbf{Y}_i|\boldsymbol{\beta}) = -\mathbf{X}_i^\top \boldsymbol{\Upsilon}_i^{-1} (\mathbf{Y}_i - \mathbf{X}_i \boldsymbol{\beta})$.
3. **Posterior predictive distribution (PPD):** For a new subject defined as, $\mathbf{Y}_{i'} = (Y_{i'1}, \dots, Y_{i'n_{i'}})^\top$, the PPD can be computed in closed form, $\mathbf{Y}_{i'}|\mathbf{Y} \sim \mathcal{N}(\mathbf{D}^{-1}\mathbf{E}, \mathbf{D}^{-1})$, where $\mathbf{D} = \boldsymbol{\Upsilon}_{i'}^{-1} - \boldsymbol{\Upsilon}_{i'}^{-1} \mathbf{X}_{i'} \mathbf{C}^{-1} \mathbf{X}_{i'}^\top \boldsymbol{\Upsilon}_{i'}^{-1}$, $\mathbf{E} = \boldsymbol{\Upsilon}_{i'}^{-1} \mathbf{X}_{i'} \mathbf{C}^{-1} \mathbf{B}$, and $\mathbf{C} = \mathbf{X}_{i'}^\top \boldsymbol{\Upsilon}_{i'}^{-1} \mathbf{X}_{i'} + \mathbf{A}$.

To compute the Monte Carlo estimator for the gradient of the marginal log-likelihood we required, $\nabla_{\boldsymbol{\beta}} \log p(\mathbf{Y}_i, \boldsymbol{\gamma}_{ir}|\boldsymbol{\beta}) = \sigma^{-2} \mathbf{X}_i^\top (\mathbf{Y}_i - \mathbf{X}_i \boldsymbol{\beta} - \mathbf{X}_i \boldsymbol{\gamma}_{ir})$ and samples of $\boldsymbol{\gamma}_{ir}$ from $\boldsymbol{\gamma}_i|\mathbf{Y}_i, \boldsymbol{\beta}$, which can be computed in closed form, $p(\boldsymbol{\gamma}_i|\mathbf{Y}_i, \boldsymbol{\beta}) = \mathcal{N}(\mathbf{F}^{-1}\mathbf{G}, \mathbf{F}^{-1})$, where $\mathbf{F} = \mathbf{X}_i^\top \mathbf{X}_i / \sigma^2 + \boldsymbol{\Sigma}^{-1}$ and $\mathbf{G} = \mathbf{X}_i^\top (\mathbf{Y}_i - \mathbf{X}_i^\top \boldsymbol{\beta}) / \sigma^2$. Throughout this simulation, we set $R = 100$. Finally, we placed a weakly informative prior on $\boldsymbol{\beta}, \boldsymbol{\beta} \sim \mathcal{N}(\mathbf{0}_p, \sigma_\beta^2 \mathbf{I}_p)$ with $\sigma_\beta^2 = 100$. The gradient with respect to this prior is given by, $\nabla_{\boldsymbol{\beta}} \log p(\boldsymbol{\beta}) = -\boldsymbol{\beta} / \sigma_\beta^2$.

Throughout this simulation, we assumed that $\mathbf{x}_{it} = (1, x_{it})^\top$ and $x_{it} \stackrel{iid}{\sim} \mathcal{N}(0, 1)$. True value of parameters were $\boldsymbol{\beta} = (1.5, -0.5)^\top$, $\sigma^2 = 2$ and $\boldsymbol{\Sigma} = \begin{pmatrix} 1.5 & -0.25 \\ -0.25 & 1.5 \end{pmatrix}$. We analyzed sample sizes of $n \in \{10^2, 10^3\}$, and set $n_i = 10$. Each algorithm was run for 100 continuous time steps (i.e., $n_{sims} = 100/\epsilon$) and thinned to yield 5,000 samples. For each setting, we simulated 100 data sets and implemented our algorithm with $S \in \{1, 5, 10\}$ and $\delta = \{\delta : \delta \in ([10]/10) \cap \epsilon = S/n^{1+\delta} < n^{-1}\}$.

Results from this simulation are presented in Figures 1 and 2 and Figures 6, 7 and 8 of the supplementary materials. In Figure 1, the log posterior variance is presented as a mean with 95% quantile intervals across the 100 simulated data sets. The results are presented for

both the uncorrected and corrected SGLD algorithm and across S , n , and parameters (β_0, β_1) and appropriate values of δ . The results indicate that the uncorrected SGLD algorithm consistently overestimated the posterior variance with estimation improving as $\delta \rightarrow 1$. As expected, when $\delta = 1$ the uncorrected SGLD properly estimated the posterior variance. Meanwhile the corrected SGLD had improved performance with quantile intervals that always include the true log variance, and the estimation improved with larger n , S , and δ . These results indicate that choosing a δ value in the middle of the range of possible δ values yields proper variance estimation. Results for posterior mean estimation are presented in supplementary Figure 6, where it can be seen that the posterior mean can be estimated properly using both the corrected and uncorrected SGLD.

Next, we explored estimation of the moments of the PPD. In Figure 2, we demonstrate the log ratio of the estimated PPD variance using either the corrected or uncorrected SGLD algorithm compared to the true PPD variance. Log ratio values near zero indicate good performance. The results are again presented across S and n and averaged across the n_i observations of $\mathbf{Y}_{i'}$. From this figure, we can see that the corrected SGLD maintains proper uncertainty quantification in the PPD in every simulation setting. The uncorrected SGLD algorithm generally performs poorly, with acceptable performance only when $\delta \rightarrow 1$. As a reminder, SGLD requires longer runtime with larger δ and when the sample size grows values of δ close to 1 are not computationally feasible. Thus, the corrected SGLD is a viable alternative to uncorrected SGLD when the sample size becomes large, because it can yield proper PPD estimation regardless of δ , and therefore is computationally efficient.

Additional results for this simulation are available in the supplementary materials. In Figure 7 of the supplementary materials, we present traceplots and density estimates for an example simulated data set to visualize the posterior variance correction. Finally, in Figure

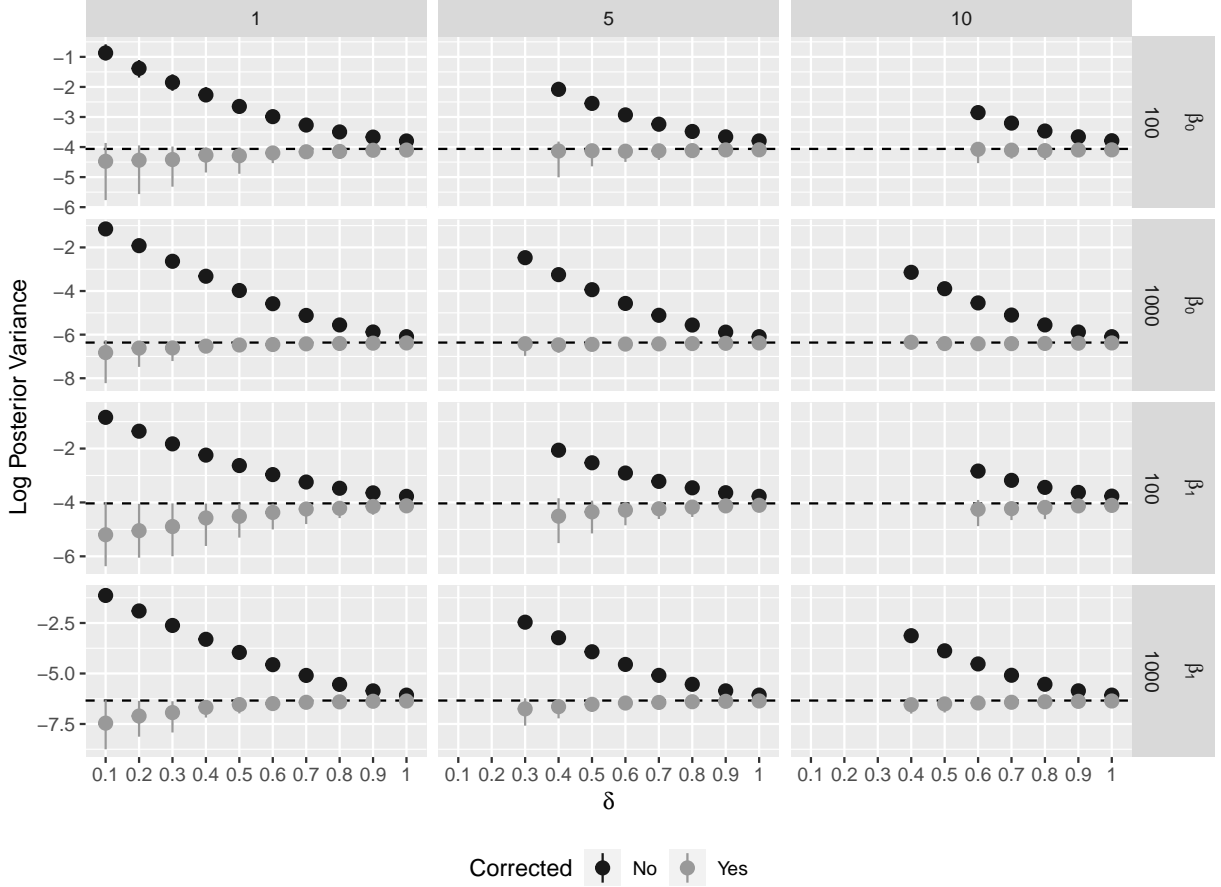


Figure 1: Posterior estimation of the log variance for uncorrected (black) and corrected (grey) SGLD algorithm. Each value represents the mean and 95% quantile intervals based on 100 simulated data sets. The columns represent the minibatch size (S) and the rows represent the sample size (n) and parameter. The black dashed lines indicate the true log posterior variance. Estimates are given across an appropriate range of δ .

8 of the supplementary materials, we present evidence that the Monte Carlo estimator does a good job of estimating the true gradient of the marginal log-likelihood (which is available in closed form in this simulation).

4.2 GLMM with Unknown Variance Components

In this section, we present simulations where the variance and dispersion parameters are unknown. In the main manuscript, we present results for the Bernoulli distribution, while

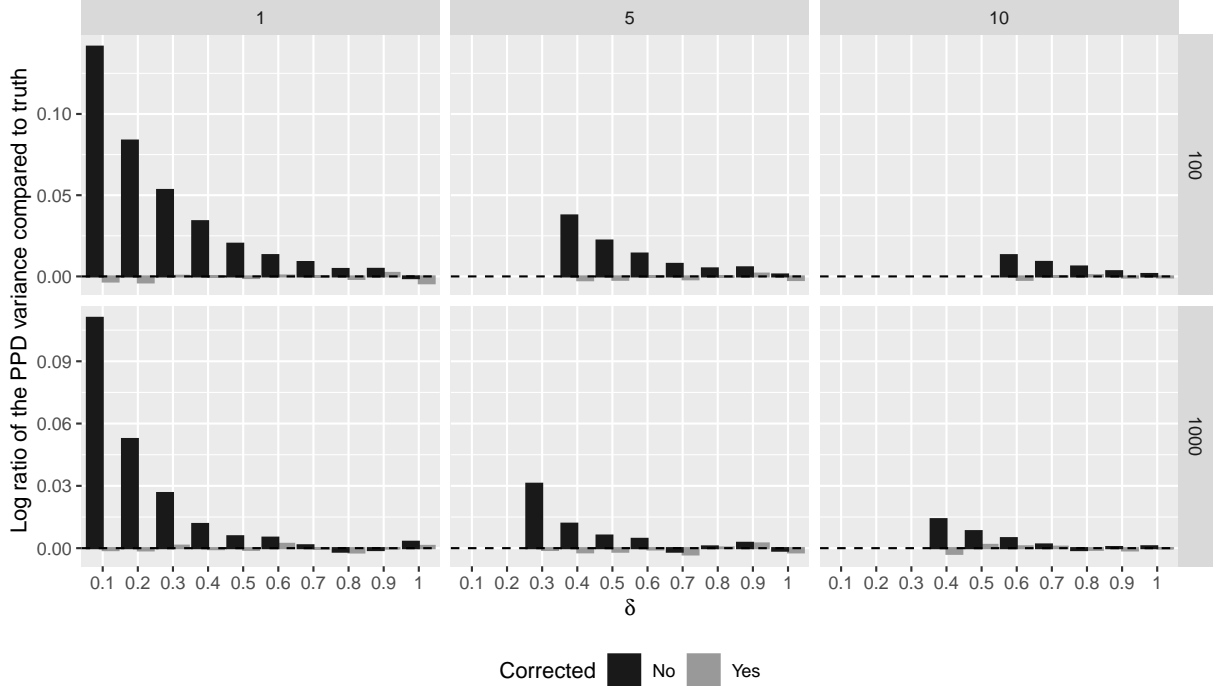


Figure 2: Assessing the algorithm’s ability to estimate the variance of the posterior predictive distribution (PPD). Presented are the log ratio of the estimated PPD variance and the true PPD variance for both the uncorrected (black) and corrected (grey) algorithms. Columns and rows indicate batch size (S) and sample size (n), respectively. Black dashed lines indicate correct PPD variance estimation. Estimates are given across a range of δ .

results for Gaussian and Poisson are reserved for the supplementary materials. The results across all distributions consistently demonstrated the utility of our algorithm.

The Bernoulli GLMM (i.e., logistic regression) is obtained from the exponential family through the following specification, $a(\phi) = 1$, $b(\theta_{it}) = \log(1 + \exp\{\theta_{it}\})$, $c(Y_{it}, \phi) = 0$, $\phi = 1$, and $\theta_{it} = \log(\pi_{it}/(1 - \pi_{it}))$. The mean parameter is given by $\mu_{it} = \pi_{it} = \exp\{\theta_{it}\}/(1 + \exp\{\theta_{it}\})$. This yields the model, $Y_{it}|\gamma_i, \Omega \stackrel{ind}{\sim} \text{Bernoulli}(\pi_{it})$, where $\text{logit}(\pi_{it}) = \mathbf{x}_{it}^\top \boldsymbol{\beta} + \mathbf{z}_{it}^\top \boldsymbol{\gamma}_i$, $\text{logit}(x) = \log(x/(1 - x))$, and the population parameters are given by, $\Omega = \{\boldsymbol{\beta}, \Sigma\}$.

We assumed that $\theta_{it} = \mathbf{x}_{it}^\top \boldsymbol{\beta} + \mathbf{x}_{it}^\top \boldsymbol{\gamma}_i$, $\mathbf{x}_{it} = (1, x_{it})^\top$ and $x_{it} \stackrel{iid}{\sim} \mathcal{N}(0, 1)$. True parameters values are the same as in Section 4.1. We examined performance for large samples sizes, $n \in \{10^4, 10^5\}$. To compare models fairly, we assessed performance as a function of runtime

and ran each model for six hours. Performance was evaluated as convergence to the proper posterior mean and variance. Since the true posterior distribution was no longer available, we compared performance to Gibbs sampling. Details for the conditional Gibbs sampler for the Bernoulli GLMM are given in Section E.1 of the supplementary materials.

We presented results for both the corrected and uncorrected SGLD algorithms for mini-batch sizes of $S \in \{1, 5, 10\}$. For each S we chose a δ using the following definition, $\delta = (\delta_{\min} + \delta_{\max})/2$, where $\delta_{\min} = \min_{\delta} \{\epsilon < n^{-1}\}$ and $\delta_{\max} = 1$ (recall that $\epsilon = n^{-(1+\delta)}S$). The intuition behind this definition is that an ideal value of δ will be in a range with proper posterior variance estimation while maximizing computational efficiency. From Figure 1 it is clear that δ in the middle of the range of possible δ values satisfies these two criteria.

4.2.1 Calculating $\nabla_{\Omega} \log p(\mathbf{Y}_i, \boldsymbol{\gamma}_{ir} | \boldsymbol{\Omega})$

To estimate the Monte Carlo gradient, we required $\nabla_{\Omega} \log p(\mathbf{Y}_i, \boldsymbol{\gamma}_{ir} | \boldsymbol{\Omega})$ with respect to each of the unconstrained parameters. Throughout the following simulations, we assumed a bivariate Gaussian for the subject-specific parameters, $p(\boldsymbol{\gamma}_i | \boldsymbol{\Sigma}) = \mathcal{N}(\mathbf{0}, \boldsymbol{\Sigma})$, where $\boldsymbol{\Sigma}$ is parameterized by the variances for the subject-specific intercept (σ_1^2) and slope (σ_2^2), and the correlation (ρ). We performed inference using the unconstrained parameters, $\delta_1 = \log(\sigma_1)$, $\delta_2 = \log(\sigma_2)$, and $\delta_{\rho} = \log((\rho + 1)/(1 - \rho))$, with corresponding gradients given by,

$$\begin{aligned} \frac{\partial \log p(\boldsymbol{\gamma}_{ir} | \boldsymbol{\Sigma})}{\partial \delta_k} &= -1 + \frac{\gamma_{irk}^2}{(1 - \rho^2)\sigma_k^2} - \frac{\rho\gamma_{ir1}\gamma_{ir2}}{(1 - \rho^2)\sigma_1\sigma_2}, \quad \text{for } k = 1, 2 \\ \frac{\partial \log p(\boldsymbol{\gamma}_{ir} | \boldsymbol{\Sigma})}{\partial \delta_{\rho}} &= \frac{\rho\sigma_1^2\sigma_2^2(1 - \rho^2) + \gamma_{ir1}\gamma_{ir2}\sigma_1\sigma_2(1 + \rho^2) - \rho\gamma_{ir2}^2\sigma_1^2 - \rho\gamma_{ir1}^2\sigma_2^2}{2\sigma_1^2\sigma_2^2(1 - \rho^2)}, \quad (13) \\ \nabla_{\boldsymbol{\Sigma}} \log p(\mathbf{Y}_i, \boldsymbol{\gamma}_{ir} | \boldsymbol{\Omega}) &= \left(\frac{\partial \log p(\boldsymbol{\gamma}_{ir} | \boldsymbol{\Sigma})}{\partial \delta_1}, \frac{\partial \log p(\boldsymbol{\gamma}_{ir} | \boldsymbol{\Sigma})}{\partial \delta_2}, \frac{\partial \log p(\boldsymbol{\gamma}_{ir} | \boldsymbol{\Sigma})}{\partial \delta_{\rho}} \right)^{\top}. \end{aligned}$$

The gradient of $\boldsymbol{\beta}$ is given in (11) and for the Bernoulli likelihood is specifically, $\nabla_{\boldsymbol{\beta}} \log p(\mathbf{Y}_i, \boldsymbol{\gamma}_{ir} | \boldsymbol{\Omega}) = \mathbf{X}_i^{\top}(\mathbf{Y}_i - \boldsymbol{\pi}_{ir})$, where $\boldsymbol{\pi}_{ir} = (\pi_{ir1}, \dots, \pi_{irn_i})^{\top}$. Together, (11) and

(13) define the relevant gradient with respect to the unconstrained parameters of Ω .

Finally, for each of the standard deviations, σ_k ($k = 1, 2$), we placed a half-t distribution with degree-of-freedom parameter ν and scale s . For a random variable x with this distribution, the gradient of the log density is given by, $\nabla_x \log p(x) = -((\nu + 1)x^2)/(s^2\nu + x^2)$. We placed a uniform prior for ρ , $\rho \sim \text{Uniform}(-1, 1)$ which yields a gradient of zero. Throughout the simulations we placed a weakly informative prior on β , $\beta \sim \mathcal{N}(\mathbf{0}_p, \sigma_\beta^2 \mathbf{I}_p)$ with $\sigma_\beta^2 = 100$. The gradient with respect to this prior is given by, $\nabla_\beta \log p(\beta) = -\beta/\sigma_\beta^2$.

4.2.2 Sampling from $p(\gamma_i | \mathbf{Y}_i, \Omega)$

To compute the Monte Carlo estimator we required samples from $p(\gamma_i | \mathbf{Y}_i, \Omega)$. We augmented the likelihood, $p(Y_{it}, \omega_{it} | \gamma_i, \Omega) = p(Y_{it} | \gamma_i, \Omega)p(\omega_{it} | \gamma_i, \Omega)$, where $\omega_{it} \sim \text{PG}(1, 0)$ is a Pólya-Gamma random variable. This likelihood permits conjugacy in γ_i and does not alter the posterior. Polson et al. (2013) showed that the likelihood could be written as, $p(Y_{it}, \omega_{it} | \gamma_i, \Omega) \propto \exp \left\{ -0.5\omega_{it} (Y_{it}^* - (\mathbf{x}_{it}^\top \beta + \mathbf{z}_{it}^\top \gamma_i))^2 \right\}$, where $\chi_{it} = Y_{it} - 0.5$ and $Y_{it}^* = \chi_{it}/\omega_{it}$. We then defined, $\mathbf{Y}_i^* = (Y_{i1}^*, \dots, Y_{in_i}^*)^\top$, $\mathbf{x}_i = (\mathbf{x}_{i1}, \dots, \mathbf{x}_{in_i})^\top$, $\mathbf{z}_i = (\mathbf{z}_{i1}, \dots, \mathbf{z}_{in_i})^\top$, $\omega_i = (\omega_{i1}, \dots, \omega_{in_i})^\top$, and $\mathbf{D}(\omega_i)$ as an $n_i \times n_i$ diagonal matrix with ω_i on the diagonal. Samples from $p(\gamma_i | \mathbf{Y}_i, \Omega)$ can be obtained by alternately sampling from the following full conditional distributions, (1) sample γ_{ir} from $\mathcal{N}(\mathbb{E}_{\gamma_i}, \mathbb{V}_{\gamma_i})$, with covariance given by $\mathbb{V}_{\gamma_i} = (\mathbf{z}_i^\top \mathbf{D}(\omega_i) \mathbf{z}_i + \Sigma^{-1})^{-1}$ and the expectation given by $\mathbb{E}_{\gamma_i} = \mathbb{V}_{\gamma_i} (\mathbf{z}_i^\top \mathbf{D}(\omega_i) (\mathbf{Y}_i^* - \mathbf{x}_i \beta))$, (2) sample ω_{it} for ($t \in [n_i]$) from $\text{PG}(1, \mathbf{x}_{it}^\top \beta + \mathbf{z}_{it}^\top \gamma_{ir})$. Due to increased complexity, $R = 1,000$.

4.2.3 Simulation results

The results for this simulation are presented in Figures 3 and 4 for the posterior mean and variance, respectively. Figure 3 presents the posterior mean estimation across runtime, where at each point in time the posterior mean was estimated using the most recent 75% of

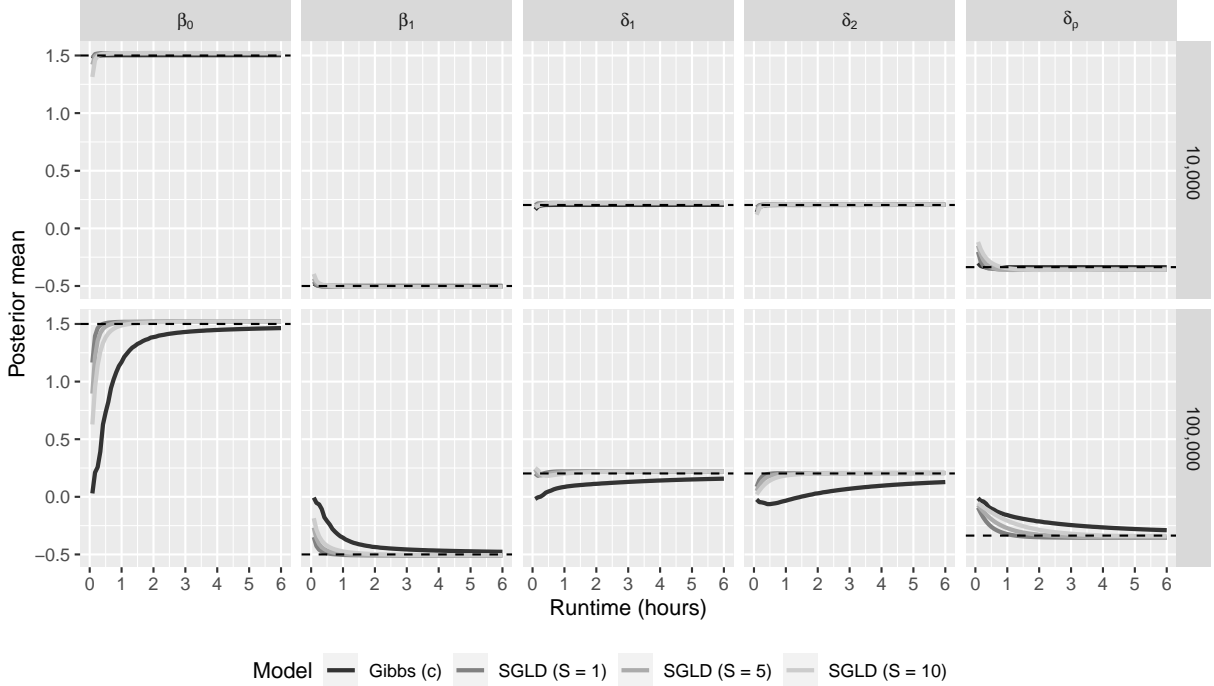


Figure 3: Posterior mean estimates presented across runtime (hours) for the Bernoulli GLMM. Columns and rows indicate parameter and sample size (n), respectively. Algorithms include the conditional (c) Gibbs sampling, and the corrected SGLD with various batch sizes (S). At each point in time, the posterior mean was calculated using the most recent 75% of the samples up to that point. Dashed black lines indicate the true value of the parameters that were used to generate the simulated data. Estimates are averaged across 100 simulated data sets.

the samples up to that point. Results are only presented for the corrected SGLD algorithm, since posterior mean estimation does not change across the corrected and uncorrected SGLD algorithms. The black dashed lines represent the values of the parameters from the data generating mechanism. For sample size of 10,000 the posterior mean was estimated nearly instantly for all of the algorithms. When the sample size increased to 100,000 the algorithms are slower to obtain the posterior mean, especially the Gibbs sampler.

Figure 4 presents posterior estimation of the variance on log scale. We cannot compare the performance to a true variance nor can we compare to the true data generating parameter values, so in this simulation the comparator becomes the Gibbs sampler. We

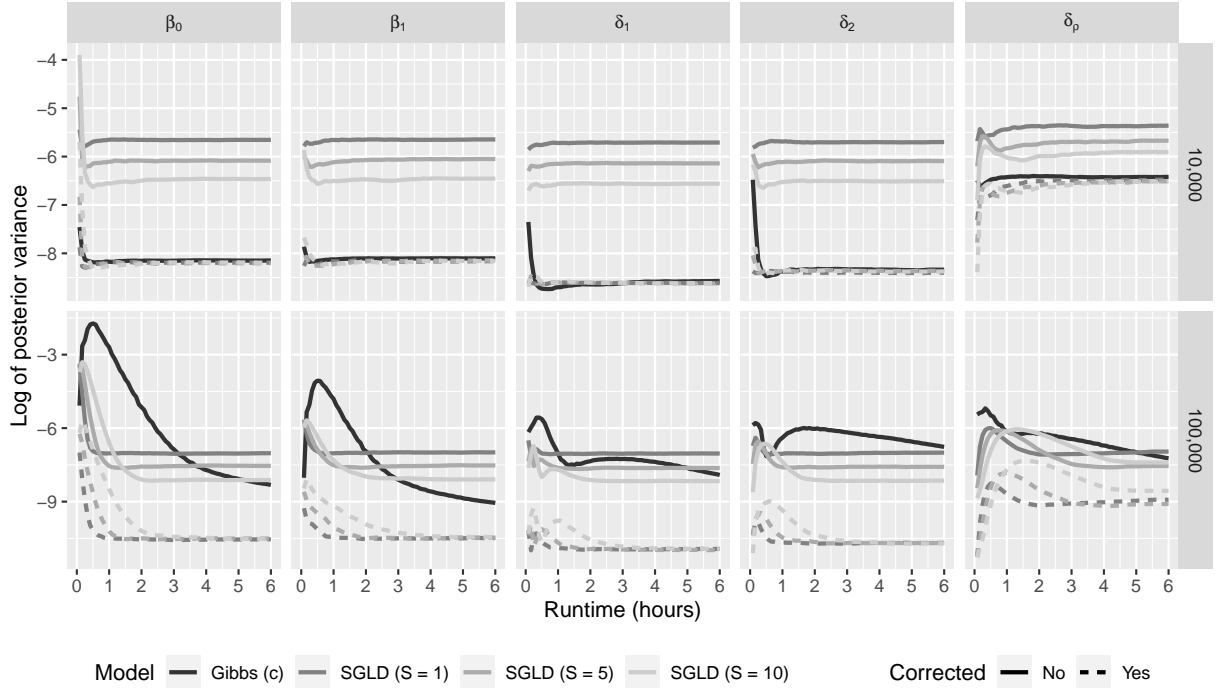


Figure 4: Log of posterior variance estimates presented across runtime (hours) for the Bernoulli GLMM model. Columns and rows indicate parameter and sample size (n), respectively. Algorithms include conditional (c) Gibbs sampling, and the SGLD algorithm with various batch sizes (S). Results are presented for both the uncorrected (solid line) and corrected (dashed line) SGLD algorithm. At each point in time, the log posterior variance was calculated using the most recent 75% of the samples up to that point. Estimates are averaged across 100 simulated data sets.

presented results for both the corrected (solid line) and uncorrected (dashed line) SGLD algorithms. To make the comparisons fair, corrections were computed during runtime, meaning $\hat{\Psi}(\Omega)$ was estimated dynamically. There are two main takeaways from this figure, (1) the corrected SGLD algorithm yielded posterior variance estimates that were the same as the Gibbs sampler algorithms, while the uncorrected SGLD algorithm overestimated the variance, and (2) the performance of the corrected SGLD algorithm was not impacted by the increase in sample size, as opposed to the Gibbs samplers whose estimation worsened. Importantly, these takeaways were true regardless of S and δ , and furthermore these results were consistent for the population regression parameters (β), and variance parameters (Σ).

Figures 9, 10, 11, and 12 in the supplementary materials present simulation results for the Gaussian, and Poisson posterior mean and variance. These results are consistent with the Bernoulli ones, and indicate the utility of our algorithm across GLMM settings.

5 Real World Data Analysis

In patients with ophthalmic disorders, psychiatric risk factors play an important role in morbidity and mortality. Understanding how patient characteristics impact the probability of a patient having distress is a critical task that will facilitate proper and early psychiatric screening and result in prompt intervention to mitigate its impact. In this analysis of real world clinical data, we analyzed data from the Duke Ophthalmic Registry, a database that consists of adults at least 18 years of age who were evaluated at the Duke Eye Center or its satellite clinics from 2012 to 2021. The goal of the analysis was to identify patient characteristics associated with a diagnosis of psychiatric distress upon each clinic encounter.

We defined $Y_{it} \in \{0, 1\}$ as an indicator of psychiatric distress for patient i ($i \in [n]$) and encounter t ($t \in [n_i]$). Distress was defined using an electronic health records phenotype that has been detailed previously (Berchuck et al., 2022). Each encounter was observed at follow-up time τ_{it} , where $\tau_{i1} = 0$, such that τ_{it} for $t > 1$ indicates the number of years from baseline encounter. The encounters for each patient were collected in the vector \mathbf{Y}_i . We also defined an indicator $w_i = 1 (\sum_{t=1}^{n_i} Y_{it} = 0)$ to indicate whether all observations for a patient were zero. The observed data is given by (\mathbf{Y}_i, w_i) with the joint distribution $p(\mathbf{Y}_i, w_i) = p(w_i)p(\mathbf{Y}_i|w_i)$. The outcome was modeled as $Y_{it} \stackrel{ind}{\sim} \text{Bernoulli}(\pi_{it})$, with $\text{logit}(\pi_{it}) = \mathbf{x}_{it}^\top \boldsymbol{\beta} + \mathbf{z}_{it}^\top \boldsymbol{\gamma}_i$ and the missing indicator was modeled as $w_i \stackrel{ind}{\sim} \text{Bernoulli}(p_i)$, where $\text{logit}(p_i) = \alpha_0 + \mathbf{x}_i^\top \boldsymbol{\alpha}_{-0}$ and $\boldsymbol{\alpha} = (\alpha_0, \boldsymbol{\alpha}_{-0}^\top)^\top$. The covariates were defined as follows, $\mathbf{x}_{it} = (1, \tau_{it}, \mathbf{x}_i^\top)$, where \mathbf{x}_i contains patient-level covariates (e.g., baseline age). The vector $\mathbf{z}_{it} = (1, \tau_{it})^\top$

inducing a subject-specific intercept and slope for follow-up time, such that $q = 2$.

The set of population parameters is $\boldsymbol{\Omega} = (\boldsymbol{\alpha}, \boldsymbol{\beta}, \boldsymbol{\Sigma})$ and the posterior distribution is, $p(\boldsymbol{\Omega}|\mathbf{Y}, \mathbf{w}) \propto p(\boldsymbol{\Omega}) \prod_{i=1}^n p(w_i|\boldsymbol{\alpha}) \int p(\mathbf{Y}_i|\boldsymbol{\gamma}_i, w_i, \boldsymbol{\beta}) p(\boldsymbol{\gamma}_i|\boldsymbol{\Sigma}) d\boldsymbol{\gamma}_i$, with corresponding gradient,

$$\nabla \log p(\boldsymbol{\Omega}|\mathbf{Y}, \mathbf{w}) = \nabla \log p(\boldsymbol{\Omega}) + \sum_{i=1}^n \nabla \log p(w_i|\boldsymbol{\alpha}) + \mathbb{E}_{\boldsymbol{\gamma}_i|\mathbf{Y}_i, w_i, \boldsymbol{\Omega}} [\nabla \log p(\mathbf{Y}_i, \boldsymbol{\gamma}_i|w_i, \boldsymbol{\Omega})],$$

where the expectation can be approximated using (6). The gradients inside of the expectation are $\nabla_{\boldsymbol{\beta}} \log p(\mathbf{Y}_i|\boldsymbol{\gamma}_{ir}, \boldsymbol{\beta}, w_i) = 1(w_i = 0) \nabla_{\boldsymbol{\beta}} \log p(\mathbf{Y}_i|\boldsymbol{\gamma}_{ir}, \boldsymbol{\beta})$, $\nabla_{\boldsymbol{\Sigma}} \log p(\boldsymbol{\gamma}_{ir}|\boldsymbol{\Sigma})$ is given by (13) and $\nabla_{\boldsymbol{\alpha}} \log p(w_i|\boldsymbol{\alpha}) = (w_i - p_i) \mathbf{x}_i^\top$. Samples of $\boldsymbol{\gamma}_{ir}$ can be obtained from $p(\boldsymbol{\gamma}_i|\mathbf{Y}_i, w_i, \boldsymbol{\Omega}) = w_i p(\boldsymbol{\gamma}_i|\boldsymbol{\Sigma}) + (1 - w_i) p(\boldsymbol{\gamma}_i|\mathbf{Y}_i, \boldsymbol{\Omega})$. It is clear that when $w_i = 1$ the posterior is equal to the prior and when $w_i = 0$ the posterior is the same as Section 4.2.2.

The sample included 40,326 patients (n), of which 15% had at least one distress indicator. On average patients had 9 encounters, were 60 years of age, 41% male, and 68% white. Full demographic details are given in Table 1 of the supplementary materials. In our model, the reference categories for categorical variables were white (Race), and commercial (Insurance). The continuous variables age, income, and education were standardized.

We performed inference using both the corrected and uncorrected SGLD algorithms using $S = 1$. In Figure 5, we presented odds ratios and 95% credible intervals for $\boldsymbol{\beta}$ for both SGLD algorithms. Estimates are color-coded to indicate whether the 95% credible interval included one, which corresponds to a one-sided Bayesian p-value. Of the variables, other race, drugs use, Medicaid insurance, Medicare insurance, single marital status, and smoking were all significantly associated with an increased probability of being distressed, assuming the presence of any distress (i.e., $w_i = 1$). An increase in baseline age, African American/black race, increased follow-up time, Hispanic/Latino ethnicity, and Asian race were all associated with a decreased probability of being distressed. Examination of this

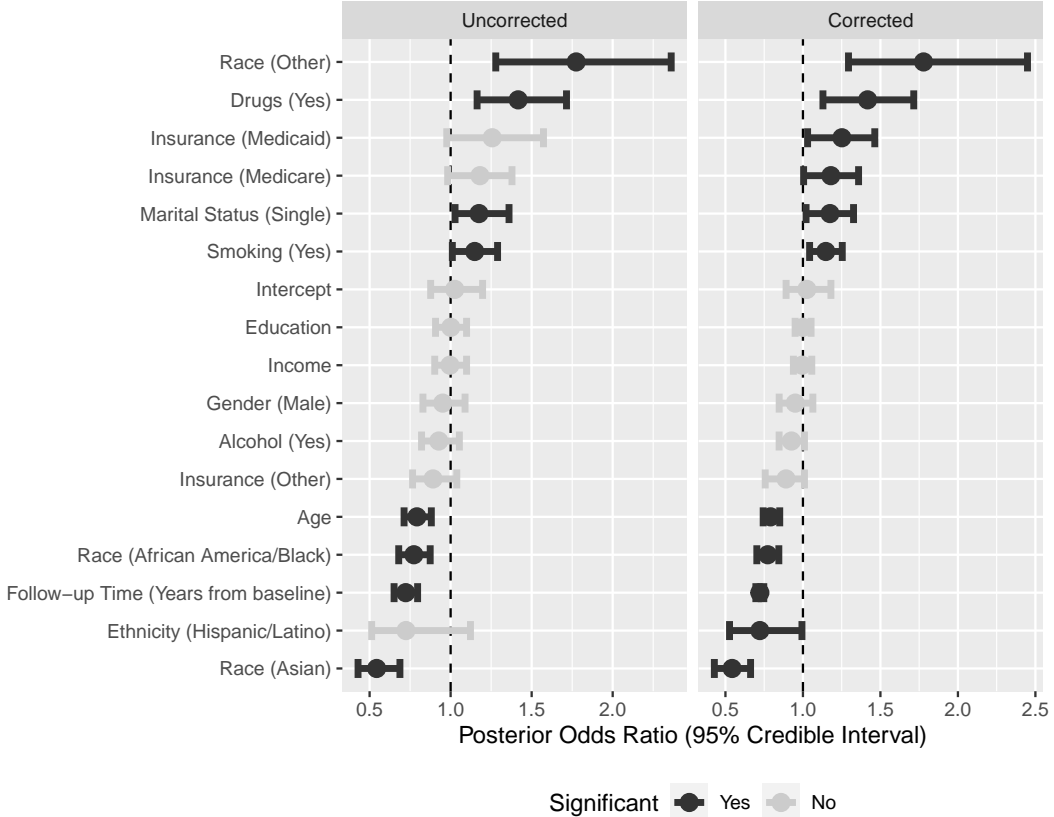


Figure 5: Posterior odds ratios and 95% credible intervals for β . Summaries are presented for the uncorrected and corrected SGLD algorithm. The parameters are presented in decreasing order and color coded based on whether the credible interval contained zero.

figure illustrates the importance of the covariance correction for obtaining proper inference as the uncorrected SGLD algorithm yielded insignificant p-values for Medicaid insurance, Medicare insurance, and Hispanic/Latino ethnicity. The posterior estimates of α and Σ are given in Figure 13 and Table 2 of the supplementary materials.

6 Discussion

In this paper, we introduced an algorithm for performing accurate and scalable Bayesian statistical inference for the GLMM in the setting of big data (i.e., as $n \rightarrow \infty$). Our algorithm lies at the intersection of AI and statistics within a SGMCMC framework. This

framework combines the machinery of modern AI algorithms to perform efficient and unbiased parameter estimation, with fully probabilistic Bayesian inference to obtain posterior samples. To the best of our knowledge, our approach is the first to adapt SGMCMC to the GLMM setting, overcoming the limitations resulting from a naive application of those methods to dependent data settings. Our main contributions include, (i) defining a convenient approximation of the gradient of the marginal log-likelihood, and (ii) an asymptotic analysis of the covariance of SGMCMC methods in the large data limit. Together, these contributions represent an extension of SGMCMC that permits efficient inference in the dependent data setting, while yielding posterior samples with proper mean and variance.

We have shown that our algorithm performs accurate and scalable inference in the GLMM setting through simulations in Section 4. In Section 4.1, we presented results for our algorithm in the linear mixed model setting with fixed variances. This simulation allowed us to compare our algorithm’s ability to recover the true posterior distribution, gradient of the marginal log-likelihood, and PPD. In Figure 1, we showed that our algorithm recovers the true posterior variance, as opposed to the uncorrected SGLD algorithm. Performance improved with larger values of S , n , and δ . These results indicate that our algorithm correctly estimates epistemic uncertainty, which is fully encoded in the posterior distribution. Thus, our algorithm permits full statistical inference, including hypothesis testing and prediction. To verify that our algorithm propagates uncertainty for prediction, we studied the moments of the PPD. In Figure 2, we presented the log ratio of the PPD variance compared to the truth for both the corrected and uncorrected SGLD algorithms. The results indicate that our covariance correction properly propagates epistemic uncertainty into the PPD for proper prediction uncertainty quantification. Our next set of simulations in Section 4.2, compared the performance of our algorithm to estimate the

posterior mean and variance to Gibbs sampling across various GLMM settings, including Bernoulli, Gaussian, and Poisson. The results consistently demonstrated that our algorithm properly estimates the posterior mean and variance and scales well as n becomes large, including settings where Gibbs sampling becomes computationally inefficient.

As noted in the introduction, it is well known that naive SGLD will lead to an inflated variance (Brosse et al., 2018), and numerous approaches have been introduced to alleviate this issue, including preconditioning (Stephan et al., 2017), however existing approaches are often computationally intensive. Our algorithm sidesteps this issue by first running the computationally efficient naive SGLD algorithm, characterizing the resulting inflated variance, and computing a *post-hoc* correction for the variance. As demonstrated in the simulations, this approach proved to be practical, as it out-performed Gibbs sampling. Note that in the setting of GLMM, when we refer to naive SGLD, we refer to SGLD without a covariance correction, but that this naive SGLD must account for the intractable marginal log-likelihood using our Monte Carlo estimator in order to be used at all.

In Section 5, we demonstrated our algorithm in a real world data analysis of electronic health records. This application presented the utility of our algorithm for performing statistical inference in complex big data settings. In Figure 5, we showed the importance of the covariance correction for statistical inference as the interpretation of the 95% credible intervals changed after the correction for insurance status and ethnicity. We note that the results we obtain critically depend on Assumption 1. In setting of model misspecification, we expect the injected noise covariance to be larger than the one obtained in simulations in the well-specified regime. Thus, a larger value of n may be needed to reach the regime studied in this paper and consequently for our computed estimates to be effective. Since some degree of model misspecification is guaranteed when working with real data, this may

explain why the correction scaling factors obtained in Figure 5 are relatively limited with respect to the values of $n^{-\delta} \approx 10^{-2}$ that one would expect from the theoretical analysis in the preceding sections. Going beyond the well-specified setting is therefore one of the main lines of future research for this work, which may be important for modeling real data.

Finally, this work opens up numerous avenues for future research. At the theoretical level, future research directions include obtaining quantitative concentration bounds for the uncorrected posterior distribution, thereby giving indications on how to choose the parameter δ based on the sample size. Additional theoretical avenues include, extending our algorithm to momentum-based SGMC methods, and to uncertainty quantification for both neural network inference and high-dimensional predictors. Methodologically, future research directions include generalizing the algorithm to allow for varying distributional assumptions and covariance specifications of the subject-specific parameters, flexible prior specification for the population regression parameter to allow for sparsity and regularization, extensions to time series or spatial data, and federated learning.

Supplementary Material

The supplementary materials contain derivations, additional simulation and data analysis results, and Gibbs sampling details.

References

Abdar, M., F. Pourpanah, S. Hussain, D. Rezazadegan, L. Liu, M. Ghavamzadeh, P. Fieguth, X. Cao, A. Khosravi, U. R. Acharya, et al. (2021). A review of uncertainty

quantification in deep learning: Techniques, applications and challenges. *Information fusion* 76, 243–297.

Agresti, A. (2012). *Categorical Data Analysis*, Volume 792. John Wiley & Sons.

Baker, J., P. Fearnhead, E. B. Fox, and C. Nemeth (2019). Control variates for stochastic gradient MCMC. *Statistics and Computing* 29, 599–615.

Berchuck, S. I., A. A. Jammal, D. Page, T. J. Somers, and F. A. Medeiros (2022). A Framework for Automating Psychiatric Distress Screening in Ophthalmology Clinics Using an EHR-Derived AI Algorithm. *Translational Vision Science & Technology* 11(10), 6–6.

Booth, J. G. and J. P. Hobert (1999). Maximizing generalized linear mixed model likelihoods with an automated monte carlo em algorithm. *Journal of the Royal Statistical Society Series B: Statistical Methodology* 61(1), 265–285.

Breslow, N. E. and D. G. Clayton (1993). Approximate inference in generalized linear mixed models. *Journal of the American Statistical Association* 88(421), 9–25.

Brosse, N., A. Durmus, and E. Moulines (2018). The promises and pitfalls of stochastic gradient Langevin dynamics. *Advances in Neural Information Processing Systems* 31, 1–11.

Casals, M., M. Girabent-Farres, and J. L. Carrasco (2014). Methodological quality and reporting of generalized linear mixed models in clinical medicine (2000–2012): A systematic review. *PloS One* 9(11), e112653.

Chen, T., E. Fox, and C. Guestrin (2014). Stochastic gradient Hamiltonian Monte Carlo. In *International Conference on Machine Learning*, pp. 1683–1691. PMLR.

Chib, S. (1995). Marginal likelihood from the gibbs output. *Journal of the American Statistical Association* 90(432), 1313–1321.

Chib, S. and I. Jeliazkov (2001). Marginal likelihood from the metropolis–hastings output. *Journal of the American Statistical Association* 96(453), 270–281.

Der Kiureghian, A. and O. Ditlevsen (2009). Aleatory or epistemic? Does it matter? *Structural Safety* 31(2), 105–112.

Fisher, R. A. (1925). Theory of Statistical Estimation. In *Mathematical Proceedings of the Cambridge Philosophical Society*, Volume 22, pp. 700–725. Cambridge University Press.

Frühwirth-Schnatter, S. (2004). Estimating marginal likelihoods for mixture and markov switching models using bridge sampling techniques. *The Econometrics Journal* 7(1), 143–167.

Gal, Y. and Z. Ghahramani (2016). Dropout as a bayesian approximation: Representing model uncertainty in deep learning. In *International Conference on Machine Learning*, pp. 1050–1059. PMLR.

Gelman, A., J. B. Carlin, H. S. Stern, and D. B. Rubin (1995). *Bayesian Data Analysis*. Chapman and Hall/CRC.

Gulshan, V., L. Peng, M. Coram, M. C. Stumpe, D. Wu, A. Narayanaswamy, S. Venugopalan, K. Widner, T. Madams, J. Cuadros, et al. (2016). Development and validation of a deep learning algorithm for detection of diabetic retinopathy in retinal fundus photographs. *JAMA* 316(22), 2402–2410.

Hüllermeier, E. and W. Waegeman (2021). Aleatoric and epistemic uncertainty in machine learning: An introduction to concepts and methods. *Machine Learning* 110, 457–506.

Jasra, A., K. J. Law, and D. Lu (2021). Unbiased estimation of the gradient of the log-likelihood in inverse problems. *Statistics and Computing* 31(3), 1–18.

Kantas, N., A. Doucet, S. S. Singh, J. Maciejowski, and N. Chopin (2015). On Particle Methods for Parameter Estimation in State-Space Models. *Statistical Science* 30(3), 328 – 351.

Kingma, D. P. and J. Ba (2017). Adam: A method for stochastic optimization.

Li, C., C. Chen, D. Carlson, and L. Carin (2016). Preconditioned stochastic gradient Langevin dynamics for deep neural networks. In *Proceedings of the AAAI Conference on Artificial Intelligence*, Volume 30.

Li, W., S. Ahn, and M. Welling (2016). Scalable MCMC for mixed membership stochastic blockmodels. In *Artificial Intelligence and Statistics*, pp. 723–731. PMLR.

Ma, Y.-A., T. Chen, and E. Fox (2015). A complete recipe for stochastic gradient MCMC. *Advances in Neural Information Processing Systems* 28, 1–9.

Ma, Y.-A., N. J. Foti, and E. B. Fox (2017). Stochastic gradient MCMC methods for hidden Markov models. In *International Conference on Machine Learning*, pp. 2265–2274. PMLR.

Matthies, H. G. (2007). Quantifying uncertainty: modern computational representation of probability and applications. In *Extreme man-made and natural hazards in dynamics of structures*, pp. 105–135. Springer.

Meza, C., F. Jaffrézic, and J.-L. Foulley (2009). Estimation in the probit normal model for binary outcomes using the SAEM algorithm. *Computational Statistics & Data Analysis* 53(4), 1350–1360.

Miller, J. W. and D. B. Dunson (2019). Robust Bayesian Inference via Coarsening. *Journal of the American Statistical Association* 114(527), 1113–1125.

Naylor, J. C. and A. F. Smith (1982). Applications of a method for the efficient computation of posterior distributions. *Journal of the Royal Statistical Society Series C: Applied Statistics* 31(3), 214–225.

Nemeth, C. and P. Fearnhead (2021). Stochastic gradient Markov chain Monte Carlo. *Journal of the American Statistical Association* 116(533), 433–450.

Ormerod, J. T. and M. P. Wand (2012). Gaussian variational approximate inference for generalized linear mixed models. *Journal of Computational and Graphical Statistics* 21(1), 2–17.

Patterson, S. and Y. W. Teh (2013). Stochastic gradient Riemannian Langevin dynamics on the probability simplex. *Advances in Neural Information Processing Systems* 26, 1–9.

Polson, N. G., J. G. Scott, and J. Windle (2013). Bayesian inference for logistic models using Pólya–Gamma latent variables. *Journal of the American Statistical Association* 108(504), 1339–1349.

Robbins, H. and S. Monro (1951). A Stochastic Approximation Method. *The Annals of Mathematical Statistics* 22(3), 400 – 407.

Rue, H., A. Riebler, S. H. Sørbye, J. B. Illian, D. P. Simpson, and F. K. Lindgren (2017). Bayesian computing with INLA: A review. *Annual Review of Statistics and Its Application* 4, 395–421.

Segal, M. and E. Weinstein (1989). A new method for evaluating the log-likelihood gradient.

ent, the Hessian, and the Fisher information matrix for linear dynamic systems. *IEEE Transactions on Information Theory* 35(3), 682–687.

Stephan, M., M. D. Hoffman, D. M. Blei, et al. (2017). Stochastic gradient descent as approximate Bayesian inference. *Journal of Machine Learning Research* 18(134), 1–35.

Tan, L. S. L. and D. J. Nott (2013). Variational Inference for Generalized Linear Mixed Models Using Partially Noncentered Parametrizations. *Statistical Science* 28(2), 168 – 188.

Teh, Y., A. Thiéry, and S. Vollmer (2016). Consistency and fluctuations for stochastic gradient Langevin dynamics. *Journal of Machine Learning Research* 17, 1–33.

Tierney, L., R. E. Kass, and J. B. Kadane (1989). Fully exponential Laplace approximations to expectations and variances of nonpositive functions. *Journal of the American Statistical Association* 84(407), 710–716.

Tran, M.-N., N. Nguyen, D. Nott, and R. Kohn (2020). Bayesian deep net GLM and GLMM. *Journal of Computational and Graphical Statistics* 29(1), 97–113.

Vollmer, S. J., K. C. Zygalakis, and Y. W. Teh (2016). Exploration of the (non-) asymptotic bias and variance of stochastic gradient Langevin dynamics. *The Journal of Machine Learning Research* 17(1), 5504–5548.

Welling, M. and Y. W. Teh (2011). Bayesian learning via stochastic gradient Langevin dynamics. In *Proceedings of the 28th international conference on machine learning (ICML-11)*, pp. 681–688.

Supplementary material to ‘Scalable Bayesian inference for the generalized linear mixed model’

This document provides supplementary material to the paper entitled ‘Scalable Bayesian inference for the generalized linear mixed model’, and is divided into six sections. Sections A, B, and C include proofs for Lemma 3.1, Lemma 3.2, and Theorem 3.5, respectively. Section D includes additional results for the simulation from Section 4.1 in the main manuscript. Section E includes additional details and results for the simulation from Section 4.2 in the main manuscript. Sections E.1, E.2, and E.3 include details on the Bernoulli, Gaussian, and Poisson GLMM simulation results. Finally, Section F includes additional results for the data analysis from Section 5 of the main manuscript.

A Proof of Lemma 3.1

In this section, we derive the first two moments for the Monte Carlo estimator for the gradient of the marginal log-likelihood for subject i , $g_i(\Omega)$, given in Lemma 3.1,

$$\hat{g}_i(\Omega) = \frac{1}{R} \sum_{r=1}^R \nabla \log p(\mathbf{Y}_i, \gamma_r | \Omega), \quad \gamma_{ir} \stackrel{\text{iid}}{\sim} p(\gamma_{ir} | \mathbf{Y}_i, \Omega).$$

We begin by denoting $g_i(\gamma | \Omega) := \nabla \log p(\mathbf{Y}_i, \gamma | \Omega)$. The estimator can be seen to be unbiased,

$$\begin{aligned} \mathbb{E}_{\gamma_i | \mathbf{Y}_i, \Omega} [\hat{g}_i(\Omega)] &= \mathbb{E}_{\gamma_i | \mathbf{Y}_i, \Omega} \left[\frac{1}{R} \sum_{r=1}^R g_i(\gamma_{ir} | \Omega) \right] \\ &= \frac{1}{R} \sum_{r=1}^R \mathbb{E}_{\gamma_i | \mathbf{Y}_i, \Omega} [g_i(\gamma_{ir} | \Omega)] \\ &= \frac{1}{R} \sum_{r=1}^R \mathbb{E}_{\gamma_i | \mathbf{Y}_i, \Omega} [g_i(\gamma_i | \Omega)] \\ &= \mathbb{E}_{\gamma_i | \mathbf{Y}_i, \Omega} [g_i(\gamma_i | \Omega)] \\ &= g_i(\Omega). \end{aligned}$$

The covariance, $\Psi_i(\Omega)$, is computed as follows,

$$\begin{aligned} \mathbb{V}_{\gamma_i | \mathbf{Y}_i, \Omega} (\hat{g}_i(\Omega)) &= \mathbb{V}_{\gamma_i | \mathbf{Y}_i, \Omega} \left(\frac{1}{R} \sum_{r=1}^R g_i(\gamma_{ir} | \Omega) \right) \\ &= \frac{1}{R^2} \mathbb{V}_{\gamma_i | \mathbf{Y}_i, \Omega} \left(\sum_{r=1}^R g_i(\gamma_{ir} | \Omega) \right) \\ &= \frac{1}{R^2} \sum_{r=1}^R \mathbb{V}_{\gamma_i | \mathbf{Y}_i, \Omega} (g_i(\gamma_{ir} | \Omega)) \\ &= \frac{1}{R} \mathbb{V}_{\gamma_i | \mathbf{Y}_i, \Omega} (g_i(\gamma_i | \Omega)) \\ &= \frac{1}{R} \mathbb{E}_{\gamma_i | \mathbf{Y}_i, \Omega} \left[(g_i(\gamma_i | \Omega) - g_i(\Omega)) (g_i(\gamma_i | \Omega) - g_i(\Omega))^{\top} \right]. \end{aligned}$$

where in the third identity we have used independence of $g_i(\boldsymbol{\gamma}_{ir}|\boldsymbol{\Omega})$ and $g_i(\boldsymbol{\gamma}_{is}|\boldsymbol{\Omega})$ for $r \neq s$.

As a reminder the estimate for the covariance is given by,

$$\hat{\boldsymbol{\Psi}}_i(\boldsymbol{\Omega}) = \frac{1}{R(R-1)} \sum_{r=1}^R (\nabla \log p(\mathbf{Y}_i, \boldsymbol{\gamma}_{ir}|\boldsymbol{\Omega}) - \hat{g}_i(\boldsymbol{\Omega})) (\nabla \log p(\mathbf{Y}_i, \boldsymbol{\gamma}_{ir}|\boldsymbol{\Omega}) - \hat{g}_i(\boldsymbol{\Omega}))^\top.$$

To prove that $\hat{\boldsymbol{\Psi}}_i(\boldsymbol{\Omega})$ is unbiased, we write,

$$\begin{aligned} (R-1)\mathbb{E}_{\boldsymbol{\gamma}_i|\mathbf{Y}_i, \boldsymbol{\Omega}} [\hat{\boldsymbol{\Psi}}_i(\boldsymbol{\Omega})] &= \mathbb{E}_{\boldsymbol{\gamma}_i|\mathbf{Y}_i, \boldsymbol{\Omega}} \left[\frac{1}{R} \sum_{r=1}^R (g_i(\boldsymbol{\gamma}_{ir}|\boldsymbol{\Omega}) - \hat{g}_i(\boldsymbol{\Omega})) (g_i(\boldsymbol{\gamma}_{ir}|\boldsymbol{\Omega}) - \hat{g}_i(\boldsymbol{\Omega}))^\top \right] \\ &= \mathbb{E}_{\boldsymbol{\gamma}_i|\mathbf{Y}_i, \boldsymbol{\Omega}} \left[(g_i(\boldsymbol{\gamma}_{i1}|\boldsymbol{\Omega}) - \hat{g}_i(\boldsymbol{\Omega})) (g_i(\boldsymbol{\gamma}_{i1}|\boldsymbol{\Omega}) - \hat{g}_i(\boldsymbol{\Omega}))^\top \right] \\ &= \mathbb{E}_{\boldsymbol{\gamma}_i|\mathbf{Y}_i, \boldsymbol{\Omega}} \left[g_i(\boldsymbol{\gamma}_{i1}|\boldsymbol{\Omega}) g_i(\boldsymbol{\gamma}_{i1}|\boldsymbol{\Omega})^\top - \frac{1}{R} \sum_{r=1}^R g_i(\boldsymbol{\gamma}_{i1}|\boldsymbol{\Omega}) g_i(\boldsymbol{\gamma}_{ir}|\boldsymbol{\Omega})^\top \right. \\ &\quad \left. - \frac{1}{R} \sum_{r=1}^R g_i(\boldsymbol{\gamma}_{ir}|\boldsymbol{\Omega}) g_i(\boldsymbol{\gamma}_{i1}|\boldsymbol{\Omega})^\top + \frac{1}{R^2} \sum_{r=1}^R \sum_{s=1}^R g_i(\boldsymbol{\gamma}_{ir}|\boldsymbol{\Omega}) g_i(\boldsymbol{\gamma}_{is}|\boldsymbol{\Omega})^\top \right] \\ &= \frac{1}{R} \left(R\mathbb{E}_{\boldsymbol{\gamma}_i|\mathbf{Y}_i, \boldsymbol{\Omega}} [g_i(\boldsymbol{\gamma}_{i1}|\boldsymbol{\Omega}) g_i(\boldsymbol{\gamma}_{i1}|\boldsymbol{\Omega})^\top] - 2(R-1)g_i(\boldsymbol{\Omega}) g_i(\boldsymbol{\Omega})^\top \right. \\ &\quad \left. - 2\mathbb{E}_{\boldsymbol{\gamma}_i|\mathbf{Y}_i, \boldsymbol{\Omega}} [g_i(\boldsymbol{\gamma}_{i1}|\boldsymbol{\Omega}) g_i(\boldsymbol{\gamma}_{i1}|\boldsymbol{\Omega})^\top] + (R-1)g_i(\boldsymbol{\Omega}) g_i(\boldsymbol{\Omega})^\top \right. \\ &\quad \left. + \mathbb{E}_{\boldsymbol{\gamma}_i|\mathbf{Y}_i, \boldsymbol{\Omega}} [g_i(\boldsymbol{\gamma}_{i1}|\boldsymbol{\Omega}) g_i(\boldsymbol{\gamma}_{i1}|\boldsymbol{\Omega})^\top] \right) \\ &= (R-1) \left(\mathbb{E}_{\boldsymbol{\gamma}_i|\mathbf{Y}_i, \boldsymbol{\Omega}} [g_i(\boldsymbol{\gamma}_{i1}|\boldsymbol{\Omega}) g_i(\boldsymbol{\gamma}_{i1}|\boldsymbol{\Omega})^\top] - g_i(\boldsymbol{\Omega}) g_i(\boldsymbol{\Omega})^\top \right) \\ &= \frac{R-1}{R} \mathbb{V}_{\boldsymbol{\gamma}_i|\mathbf{Y}_i, \boldsymbol{\Omega}} (g_i(\boldsymbol{\gamma}_{i1}|\boldsymbol{\Omega})) = (R-1)\boldsymbol{\Psi}_i(\boldsymbol{\Omega}). \end{aligned}$$

□

B Proof for Lemma 3.2

We are interested in defining the first two moments of $\bar{g}_{\mathcal{S}}(\boldsymbol{\Omega}) = \sum_{i \in \mathcal{S}} \hat{g}_i(\boldsymbol{\Omega}) / S$. Note that the moments are computed with respect to the Monte Carlo estimator and the observed data. We begin by showing that $\bar{g}_{\mathcal{S}}(\boldsymbol{\Omega})$ is an unbiased estimator of $\bar{g}_n(\boldsymbol{\Omega}) = \sum_{i=1}^n g_i(\boldsymbol{\Omega}) / n = \mathbb{E}_{\mathbf{Y}_i} [g_i(\boldsymbol{\Omega})]$,

$$\begin{aligned}
\mathbb{E}_{\mathbf{Y}_i, \hat{g}_i(\boldsymbol{\Omega})}^{\otimes S} [\bar{g}_{\mathcal{S}}(\boldsymbol{\Omega})] &= \mathbb{E}_{\mathbf{Y}_i} \left[\mathbb{E}_{\hat{g}_i(\boldsymbol{\Omega}) | \mathbf{Y}_i} \left[\frac{1}{S} \sum_{i \in \mathcal{S}} \hat{g}_i(\boldsymbol{\Omega}) \right] \right] \\
&= \frac{1}{S} \sum_{i \in \mathcal{S}} \mathbb{E}_{\mathbf{Y}_i} [\mathbb{E}_{\hat{g}_i(\boldsymbol{\Omega}) | \mathbf{Y}_i} [\hat{g}_i(\boldsymbol{\Omega})]] \\
&= \frac{1}{S} \sum_{i \in \mathcal{S}} \mathbb{E}_{\mathbf{Y}_i} [g_i(\boldsymbol{\Omega})] \\
&= \frac{1}{S} \sum_{i \in \mathcal{S}} \bar{g}_n(\boldsymbol{\Omega}) \\
&= \bar{g}_n(\boldsymbol{\Omega}),
\end{aligned}$$

where $\mathbb{E}_{\mathbf{Y}_i, \hat{g}_i(\boldsymbol{\Omega})}^{\otimes S}$ indicates that the expectation is taken with respect to the pair $(\mathbf{Y}_i, \hat{g}_i(\boldsymbol{\Omega}))$ for all $i \in \mathcal{S}$. Note that we suppress the dependence of the expectation with respect to $\boldsymbol{\gamma}_{ir} | \mathbf{Y}_i, \boldsymbol{\Omega}$, since the randomness is encoded in $\hat{g}_i(\boldsymbol{\Omega})$.

Next, we proceed to derive the covariance of $\bar{g}_{\mathcal{S}}(\boldsymbol{\Omega})$. Before this, we define $\bar{\Psi}_n(\boldsymbol{\Omega}) = \mathbb{E}_{\mathbf{Y}_i} [\Psi_i(\boldsymbol{\Omega})] = \sum_{i=1}^n \Psi_i(\boldsymbol{\Omega}) / n$ and

$$\begin{aligned}
\bar{\Phi}_n(\boldsymbol{\Omega}) &= \mathbb{V}_{\mathbf{Y}_i} (g_i(\boldsymbol{\Omega})) \\
&= \mathbb{E}_{\mathbf{Y}_i} \left[(g_i(\boldsymbol{\Omega}) - \mathbb{E}_{\mathbf{Y}_i} [g_i(\boldsymbol{\Omega})]) (g_i(\boldsymbol{\Omega}) - \mathbb{E}_{\mathbf{Y}_i} [g_i(\boldsymbol{\Omega})])^\top \right] \\
&= \frac{1}{n} \sum_{i=1}^n (g_i(\boldsymbol{\Omega}) - \bar{g}_n(\boldsymbol{\Omega})) (g_i(\boldsymbol{\Omega}) - \bar{g}_n(\boldsymbol{\Omega}))^\top.
\end{aligned}$$

The normalized covariance of $\bar{g}_{\mathcal{S}}(\boldsymbol{\Omega})$ can then be computed as follows,

$$\begin{aligned}
S\Psi(\boldsymbol{\Omega}) &= S\mathbb{V}_{\mathbf{Y}_i, \hat{g}_i(\boldsymbol{\Omega})}^{\otimes S}(\bar{g}_{\mathcal{S}}(\boldsymbol{\Omega})) \\
&= S\mathbb{V}_{\mathbf{Y}_i, \hat{g}_i(\boldsymbol{\Omega})}^{\otimes S}\left(\frac{1}{S} \sum_{i \in \mathcal{S}} \hat{g}_i(\boldsymbol{\Omega})\right) \\
&= \frac{1}{S} \sum_{i \in \mathcal{S}} \mathbb{V}_{\mathbf{Y}_i, \hat{g}_i(\boldsymbol{\Omega})}(\hat{g}_i(\boldsymbol{\Omega})) \\
&= \frac{1}{S} \sum_{i \in \mathcal{S}} \mathbb{V}_{\mathbf{Y}_i}(\mathbb{E}_{\hat{g}_i(\boldsymbol{\Omega})|\mathbf{Y}_i}[\hat{g}_i(\boldsymbol{\Omega})]) + \mathbb{E}_{\mathbf{Y}_i}[\mathbb{V}_{\hat{g}_i(\boldsymbol{\Omega})|\mathbf{Y}_i}(\hat{g}_i(\boldsymbol{\Omega}))] \\
&= \frac{1}{S} \sum_{i \in \mathcal{S}} \mathbb{V}_{\mathbf{Y}_i}(g_i(\boldsymbol{\Omega})) + \mathbb{E}_{\mathbf{Y}_i}[\Psi_i(\boldsymbol{\Omega})] \\
&= \frac{1}{S} \sum_{i \in \mathcal{S}} \bar{\Phi}_n(\boldsymbol{\Omega}) + \bar{\Psi}_n(\boldsymbol{\Omega}) \\
&= \bar{\Phi}_n(\boldsymbol{\Omega}) + \bar{\Psi}_n(\boldsymbol{\Omega}) \\
&= \frac{1}{n} \sum_{i=1}^n (g_i(\boldsymbol{\Omega}) - \bar{g}_n(\boldsymbol{\Omega})) (g_i(\boldsymbol{\Omega}) - \bar{g}_n(\boldsymbol{\Omega}))^\top + \Psi_i(\boldsymbol{\Omega}),
\end{aligned}$$

where $\bar{g}_n(\boldsymbol{\Omega}) = \frac{1}{n} \sum_{i=1}^n g_i(\boldsymbol{\Omega})$. Finally, we show that $\hat{\Psi}(\boldsymbol{\Omega})$ is an unbiased estimator of $\Psi(\boldsymbol{\Omega})$. We begin by writing the following, quantity,

$$\begin{aligned}
\hat{\Psi}(\boldsymbol{\Omega}) &= \hat{\Phi}_n(\boldsymbol{\Omega}) + \hat{\Psi}_n(\boldsymbol{\Omega}) \\
&= \frac{1}{n} \sum_{i=1}^n (\hat{g}_i(\boldsymbol{\Omega}) - \hat{\bar{g}}_n(\boldsymbol{\Omega})) (\hat{g}_i(\boldsymbol{\Omega}) - \hat{\bar{g}}_n(\boldsymbol{\Omega}))^\top + \frac{\hat{\Psi}_i(\boldsymbol{\Omega})}{n},
\end{aligned}$$

where $\hat{\Phi}_n(\boldsymbol{\Omega}) = \sum_{i=1}^n (\hat{g}_i(\boldsymbol{\Omega}) - \hat{\bar{g}}_n(\boldsymbol{\Omega})) (\hat{g}_i(\boldsymbol{\Omega}) - \hat{\bar{g}}_n(\boldsymbol{\Omega}))^\top / n$, $\hat{\Psi}_n(\boldsymbol{\Omega}) = \sum_{i=1}^n \hat{\Psi}_i(\boldsymbol{\Omega}) / n^2$, and $\hat{\bar{g}}_n(\boldsymbol{\Omega}) = \sum_{i=1}^n \hat{g}_i(\boldsymbol{\Omega}) / n$. To show $\hat{\Psi}(\boldsymbol{\Omega})$ is an unbiased estimator of $\Psi(\boldsymbol{\Omega})$, we derive the following two identities,

$$n\mathbb{E}_{\mathbf{Y}_i, \hat{g}_i(\boldsymbol{\Omega})}^{\otimes n} \left[\hat{\Psi}_n(\boldsymbol{\Omega}) \right] = \mathbb{E}_{\mathbf{Y}_i, \hat{g}_i(\boldsymbol{\Omega})}^{\otimes n} \left[\frac{1}{n} \sum_{i=1}^n \hat{\Psi}_i(\boldsymbol{\Omega}) \right]$$

$$\begin{aligned}
&= \frac{1}{n} \sum_{i=1}^n \mathbb{E}_{\mathbf{Y}_i} \left[\mathbb{E}_{\hat{g}_i(\boldsymbol{\Omega})|\mathbf{Y}_i} \left[\hat{\Psi}_i(\boldsymbol{\Omega}) \right] \right] \\
&= \frac{1}{n} \sum_{i=1}^n \mathbb{E}_{\mathbf{Y}_i} [\Psi_i(\boldsymbol{\Omega})] \\
&= \frac{1}{n} \sum_{i=1}^n \bar{\Psi}_n(\boldsymbol{\Omega}) \\
&= \bar{\Psi}_n(\boldsymbol{\Omega}),
\end{aligned}$$

and,

$$\begin{aligned}
\mathbb{E}_{\mathbf{Y}_i, \hat{g}_i(\boldsymbol{\Omega})}^{\otimes n} \left[\hat{\Phi}_n(\boldsymbol{\Omega}) \right] &= \mathbb{E}_{\mathbf{Y}_i, \hat{g}_i(\boldsymbol{\Omega})}^{\otimes n} \left[\frac{1}{n} \sum_{i=1}^n (\hat{g}_i(\boldsymbol{\Omega}) - \hat{g}_n(\boldsymbol{\Omega})) (\hat{g}_i(\boldsymbol{\Omega}) - \hat{g}_n(\boldsymbol{\Omega}))^\top \right] \\
&= \mathbb{E}_{\mathbf{Y}_i}^{\otimes n} \left[\mathbb{E}_{\hat{g}_i(\boldsymbol{\Omega})|\mathbf{Y}_i}^{\otimes n} \left[\frac{1}{n} \sum_{i=1}^n (\hat{g}_i(\boldsymbol{\Omega}) - \hat{g}_n(\boldsymbol{\Omega})) (\hat{g}_i(\boldsymbol{\Omega}) - \hat{g}_n(\boldsymbol{\Omega}))^\top \right] \right] \\
&= \frac{1}{n} \sum_{i=1}^n \mathbb{E}_{\hat{g}_i(\boldsymbol{\Omega})|\mathbf{Y}_i}^{\otimes n} \left[(\hat{g}_i(\boldsymbol{\Omega}) - \hat{g}_n(\boldsymbol{\Omega})) (\hat{g}_i(\boldsymbol{\Omega}) - \hat{g}_n(\boldsymbol{\Omega}))^\top \right] \\
&= \frac{1}{n} \sum_{i=1}^n \mathbb{E}_{\hat{g}_i(\boldsymbol{\Omega})|\mathbf{Y}_i}^{\otimes n} \left[\hat{g}_i(\boldsymbol{\Omega}) \hat{g}_i(\boldsymbol{\Omega})^\top \right] - \frac{1}{n} \mathbb{E}_{\hat{g}_i(\boldsymbol{\Omega})|\mathbf{Y}_i}^{\otimes n} \left[\hat{g}_i(\boldsymbol{\Omega}) \left(\frac{1}{n} \sum_{j=1}^n \hat{g}_j(\boldsymbol{\Omega}) \right)^\top \right] \\
&\quad - \frac{1}{n} \mathbb{E}_{\hat{g}_i(\boldsymbol{\Omega})|\mathbf{Y}_i}^{\otimes n} \left[\left(\frac{1}{n} \sum_{k=1}^n \hat{g}_k(\boldsymbol{\Omega}) \right) \hat{g}_i(\boldsymbol{\Omega})^\top \right] + \frac{1}{n^2} \sum_{j=1}^n \sum_{k=1}^n \mathbb{E}_{\hat{g}_i(\boldsymbol{\Omega})|\mathbf{Y}_i}^{\otimes n} \left[\hat{g}_j(\boldsymbol{\Omega}) \hat{g}_k(\boldsymbol{\Omega})^\top \right] \\
&= \frac{1}{n} \sum_{i=1}^n \mathbb{E}_{\hat{g}_i(\boldsymbol{\Omega})|\mathbf{Y}_i}^{\otimes n} \left[\hat{g}_i(\boldsymbol{\Omega}) \hat{g}_i(\boldsymbol{\Omega})^\top \right] - \frac{1}{n^2} \mathbb{E}_{\hat{g}_i(\boldsymbol{\Omega})|\mathbf{Y}_i}^{\otimes n} \left[\hat{g}_i(\boldsymbol{\Omega}) \left(\hat{g}_i(\boldsymbol{\Omega}) + \sum_{j \neq i} \hat{g}_j(\boldsymbol{\Omega}) \right)^\top \right] \\
&\quad - \frac{1}{n^2} \mathbb{E}_{\hat{g}_i(\boldsymbol{\Omega})|\mathbf{Y}_i}^{\otimes n} \left[\left(\hat{g}_i(\boldsymbol{\Omega}) + \sum_{k \neq i} \hat{g}_k(\boldsymbol{\Omega}) \right) \hat{g}_i(\boldsymbol{\Omega})^\top \right] + \frac{1}{n^2} \sum_{j=1}^n \mathbb{E}_{\hat{g}_i(\boldsymbol{\Omega})|\mathbf{Y}_i}^{\otimes n} \left[\hat{g}_j(\boldsymbol{\Omega}) \hat{g}_j(\boldsymbol{\Omega})^\top \right] \\
&= \frac{1}{n} \sum_{i=1}^n \mathbb{E}_{\hat{g}_i(\boldsymbol{\Omega})|\mathbf{Y}_i}^{\otimes n} \left[\hat{g}_i(\boldsymbol{\Omega}) \hat{g}_i(\boldsymbol{\Omega})^\top \right] - \frac{2}{n^2} \sum_{i=1}^n \mathbb{E}_{\hat{g}_i(\boldsymbol{\Omega})|\mathbf{Y}_i}^{\otimes n} \left[\hat{g}_i(\boldsymbol{\Omega}) \hat{g}_i(\boldsymbol{\Omega})^\top \right] \\
&\quad + \frac{1}{n^2} \sum_{i=1}^n \mathbb{E}_{\hat{g}_i(\boldsymbol{\Omega})|\mathbf{Y}_i}^{\otimes n} \left[\hat{g}_i(\boldsymbol{\Omega}) \hat{g}_i(\boldsymbol{\Omega})^\top \right] - \frac{2}{n} \sum_{j \neq k} g_j(\boldsymbol{\Omega}) g_k(\boldsymbol{\Omega})^\top + \frac{1}{n^2} \sum_{j \neq k} g_j(\boldsymbol{\Omega}) g_k(\boldsymbol{\Omega})^\top \\
&= \frac{n-1}{n^2} \sum_{i=1}^n \mathbb{E}_{\hat{g}_i(\boldsymbol{\Omega})|\mathbf{Y}_i}^{\otimes n} \left[\hat{g}_i(\boldsymbol{\Omega}) \hat{g}_i(\boldsymbol{\Omega})^\top \right] - \frac{1}{n^2} \sum_{j \neq k} g_j(\boldsymbol{\Omega}) g_k(\boldsymbol{\Omega})^\top \\
&= \frac{n-1}{n^2} \sum_{i=1}^n \mathbb{E}_{\hat{g}_i(\boldsymbol{\Omega})|\mathbf{Y}_i}^{\otimes n} \left[\hat{g}_i(\boldsymbol{\Omega}) \hat{g}_i(\boldsymbol{\Omega})^\top - g_i(\boldsymbol{\Omega}) g_i(\boldsymbol{\Omega})^\top \right] + \frac{n-1}{n^2} \sum_{i=1}^n g_i(\boldsymbol{\Omega}) g_i(\boldsymbol{\Omega})^\top
\end{aligned}$$

$$\begin{aligned}
& -\frac{1}{n^2} \sum_{j \neq k} g_j(\boldsymbol{\Omega}) g_k(\boldsymbol{\Omega})^\top \\
& = \frac{n-1}{n^2} \sum_{i=1}^n \mathbb{E}_{\hat{g}_i(\boldsymbol{\Omega}) \mid \mathbf{Y}_i} [\hat{g}_i(\boldsymbol{\Omega}) \hat{g}_i(\boldsymbol{\Omega})^\top - g_i(\boldsymbol{\Omega}) g_i(\boldsymbol{\Omega})^\top] + \frac{1}{n} \sum_{i=1}^n g_i(\boldsymbol{\Omega}) g_i(\boldsymbol{\Omega})^\top \\
& \quad - \frac{1}{n^2} \sum_{j=1}^n \sum_{k=1}^n g_j(\boldsymbol{\Omega}) g_k(\boldsymbol{\Omega})^\top \\
& = \frac{n-1}{n} \left(\frac{1}{n} \sum_{i=1}^n \boldsymbol{\Psi}_i(\boldsymbol{\Omega}) \right) + \frac{1}{n} \sum_{i=1}^n (g_i(\boldsymbol{\Omega}) - \bar{g}_n(\boldsymbol{\Omega})) (g_i(\boldsymbol{\Omega}) - \bar{g}_n(\boldsymbol{\Omega}))^\top \\
& = \left(1 - \frac{1}{n} \right) \bar{\boldsymbol{\Psi}}_n(\boldsymbol{\Omega}) + \bar{\boldsymbol{\Phi}}_n(\boldsymbol{\Omega}).
\end{aligned}$$

Then, we have,

$$\begin{aligned}
\mathbb{E}_{\mathbf{Y}_i, \hat{g}_i(\boldsymbol{\Omega})}^{\otimes n} [\hat{\boldsymbol{\Psi}}_n(\boldsymbol{\Omega})] & = \mathbb{E}_{\mathbf{Y}_i, \hat{g}_i(\boldsymbol{\Omega})}^{\otimes n} [\hat{\bar{\boldsymbol{\Phi}}}_n(\boldsymbol{\Omega}) + \hat{\bar{\boldsymbol{\Psi}}}_n(\boldsymbol{\Omega})] \\
& = \mathbb{E}_{\mathbf{Y}_i, \hat{g}_i(\boldsymbol{\Omega})}^{\otimes n} [\hat{\bar{\boldsymbol{\Phi}}}_n(\boldsymbol{\Omega})] + \mathbb{E}_{\mathbf{Y}_i, \hat{g}_i(\boldsymbol{\Omega})}^{\otimes n} [\hat{\bar{\boldsymbol{\Psi}}}_n(\boldsymbol{\Omega})] \\
& = \left(1 - \frac{1}{n} \right) \bar{\boldsymbol{\Psi}}_n(\boldsymbol{\Omega}) + \bar{\boldsymbol{\Phi}}_n(\boldsymbol{\Omega}) + \frac{\bar{\boldsymbol{\Psi}}_n(\boldsymbol{\Omega})}{n} \\
& = \bar{\boldsymbol{\Psi}}_n(\boldsymbol{\Omega}) + \bar{\boldsymbol{\Phi}}_n(\boldsymbol{\Omega}) \\
& = \boldsymbol{\Psi}(\boldsymbol{\Omega}).
\end{aligned}$$

□

C Proof of Theorem 3.5

Let Ω_0 be distributed according to $\tilde{\pi}$ and define $\xi_k(\Omega) := n/\sqrt{S}\xi_k(\Omega)$. By the definition of the SGLD update, using a Taylor expansion around Ω^* for ∇f , we obtain,

$$\Omega_1 - \Omega^* = \Omega_0 - \Omega^* - \epsilon(\nabla^2 f(\Omega^*)(\Omega_0 - \Omega^*) + R_1(\Omega_0) + \xi'_0(\Omega_0)) + \kappa\sqrt{2\epsilon}Z_1,$$

where by Assumption 1, $R_1 : \mathbb{R}^d \rightarrow \mathbb{R}^d$ satisfies

$$\sup_{\Omega \in \mathbb{R}^d} \frac{\|R_1(\Omega)\|}{\|\Omega - \Omega^*\|^2} \leq L/2. \quad (14)$$

Taking a product and the expectation, and using that Ω_0 , ξ'_0 , Z_1 are mutually independent, we obtain

$$\begin{aligned} & \mathbb{E}[\nabla^2 f(\Omega^*)(\Omega_0 - \Omega^*)(\Omega_0 - \Omega^*)^\top + (\Omega_0 - \Omega^*)(\Omega_0 - \Omega^*)^\top \nabla^2 f(\Omega^*)] \quad (15) \\ &= 2\kappa \text{Id} + \epsilon \mathbb{E}[\xi'_0(\Omega_0) \xi'_0(\Omega_0)^\top] \\ &+ \mathbb{E}[(R_1(\Omega_0) + \xi'_0(\Omega_0))(\Omega_0 - \Omega^*)^\top + (\Omega_0 - \Omega^*)(R_1(\Omega_0) + \xi'_0(\Omega_0))^\top] \\ &+ \epsilon \mathbb{E}[R_1(\Omega_0)^2 + \nabla^2 f(\Omega^*)(\Omega_0 - \Omega^*)(R_1(\Omega_0) + \xi'_0(\Omega_0))^\top \\ &+ (R_1(\Omega_0) + \xi'_0(\Omega_0)) \nabla^2 f(\Omega^*)(\Omega_0 - \Omega^*)]. \end{aligned}$$

Now, by a Taylor expansion of ξ'_0 around Ω^* , we get for all $\Omega \in \mathbb{R}^d$, \mathbb{P} -almost-surely,

$$\xi'_0(\Omega) = \xi'_0(\Omega^*) + \nabla \xi'_0(\Omega^*)(\Omega - \Omega^*) + R_2(\Omega),$$

where by Assumption 1, $R_2 : \mathbb{R}^d \rightarrow \mathbb{R}^d$ satisfies

$$\sup_{\Omega \in \mathbb{R}^d} \frac{\|R_2(\Omega)\|}{\|\Omega - \Omega^*\|^2} \leq L/2. \quad (16)$$

Therefore, taking the tensor product and the expectation, we obtain

$$\mathbb{E}[\xi'_0(\Omega_0)\xi'_0(\Omega_0)^\top] = \mathbb{E}[\xi'_0(\Omega^*)\xi'_0(\Omega^*)^\top] + \mathbb{E}[R_3(\Omega_0)]$$

where

$$\mathbb{E}[\xi'_0(\Omega^*)\xi'_0(\Omega^*)^\top] = \frac{n^2}{S}\Psi(\Omega^*) \quad (17)$$

$R_3 : \mathbb{R}^d \rightarrow \mathbb{R}^{d \times d}$ is defined for all $\Omega \in \mathbb{R}^d$, \mathbb{P} -almost-surely,

$$\begin{aligned} R_3(\Omega) &= \nabla \xi'_0(\Omega^*)(\Omega - \Omega^*)(\nabla \xi'_0(\Omega^*)(\Omega - \Omega^*))^\top \\ &\quad + \xi'_0(\Omega^*)(\nabla \xi'_0(\Omega^*)(\Omega - \Omega^*))^\top + \nabla \xi'_0(\Omega^*)(\Omega - \Omega^*)\xi'_0(\Omega^*)^\top \\ &\quad + (\xi'_0(\Omega^*) + \nabla \xi'_0(\Omega^*)(\Omega - \Omega^*))R_2(\Omega)^\top \\ &\quad + R_2(\Omega)(\xi'_0(\Omega^*) + \nabla \xi'_0(\Omega^*)(\Omega - \Omega^*))^\top \\ &\quad + R_2(\Omega)R_2(\Omega)^\top = O_n(n^{1-5\delta/4}) \end{aligned}$$

where in the last equality we have combined Cauchy-Schwarz inequality with (16) and (Brosse et al., 2018, Corollary 3 ii)), which adapted to our setting states that

$$\mathbb{E}[\|\Omega - \Omega^*\|^4] = O_n(n^{-2\delta}).$$

Combining this fact, (14) and (17) with (15) yields the desired bound. \square

D Additional details on Simulation 4.1

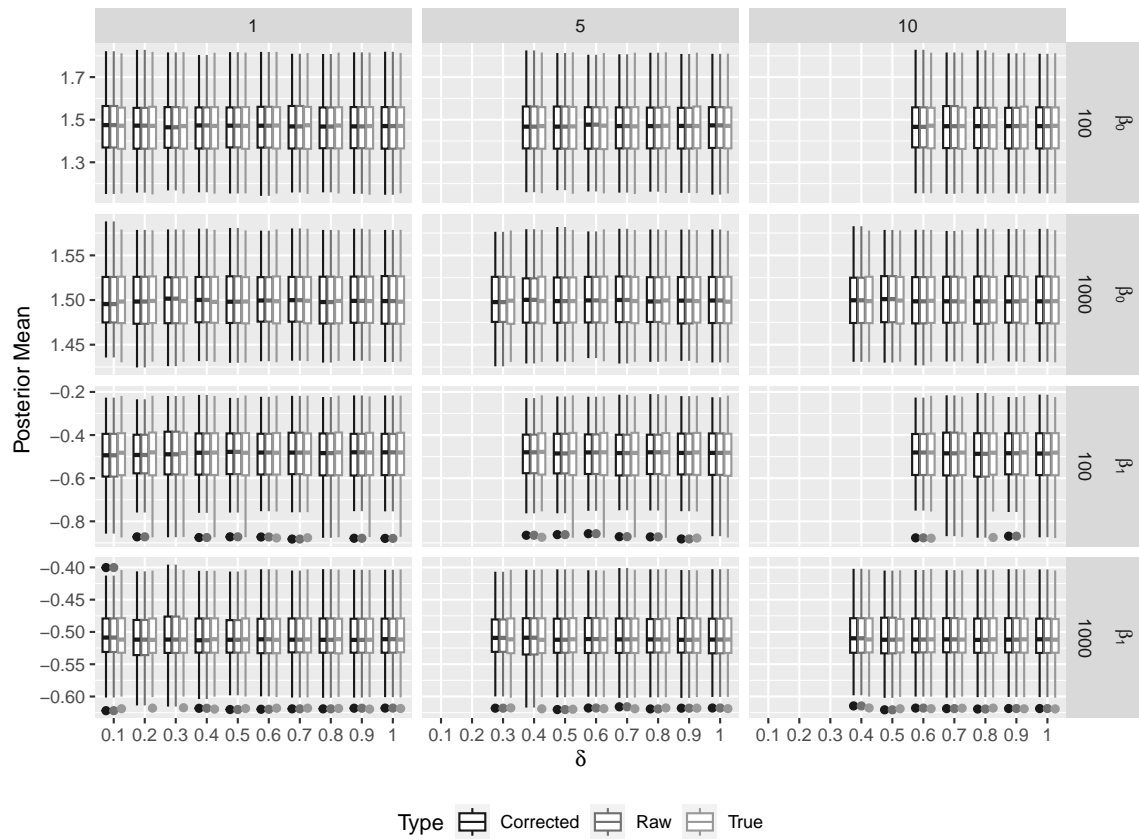


Figure 6: Posterior mean estimation for corrected and uncorrected SGLD algorithm and the true posterior. Histograms represent the posterior mean from the 100 simulated data sets. The columns represent the minibatch size (S) and the rows represent the sample size (n) and parameter. Estimates are given across an appropriate range of δ .

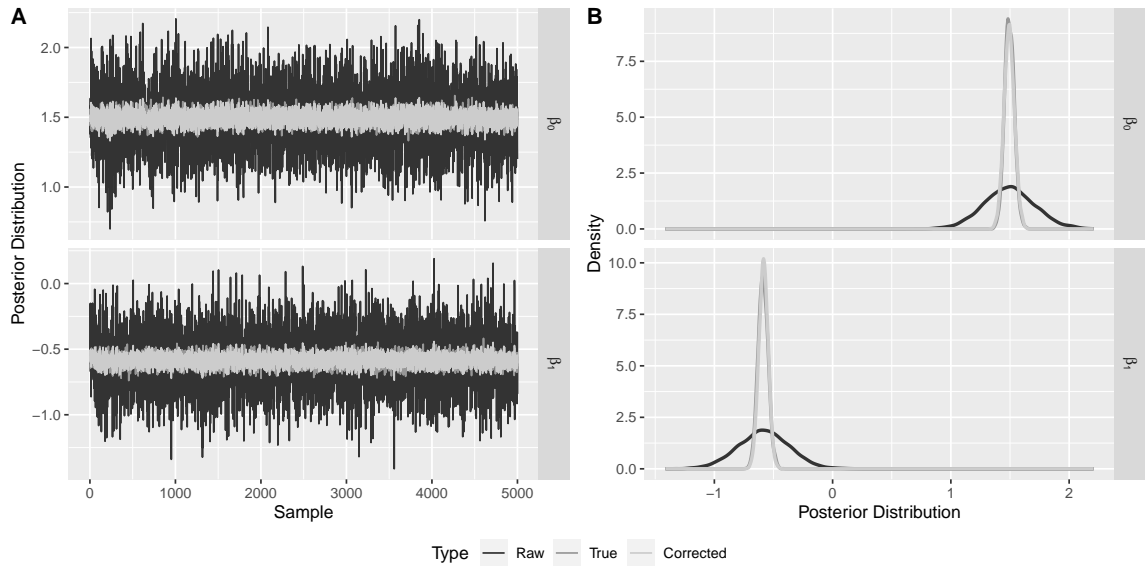


Figure 7: Traceplots (A) and density plots (B) of the posterior distributions for the raw uncorrected SGLD algorithm (black), the true posterior (dark grey), and the corrected SGLD algorithm (light grey). These results are presented for a simulated data set where $n = 10^3$, $S = 10$, and $\delta = 0.4$.

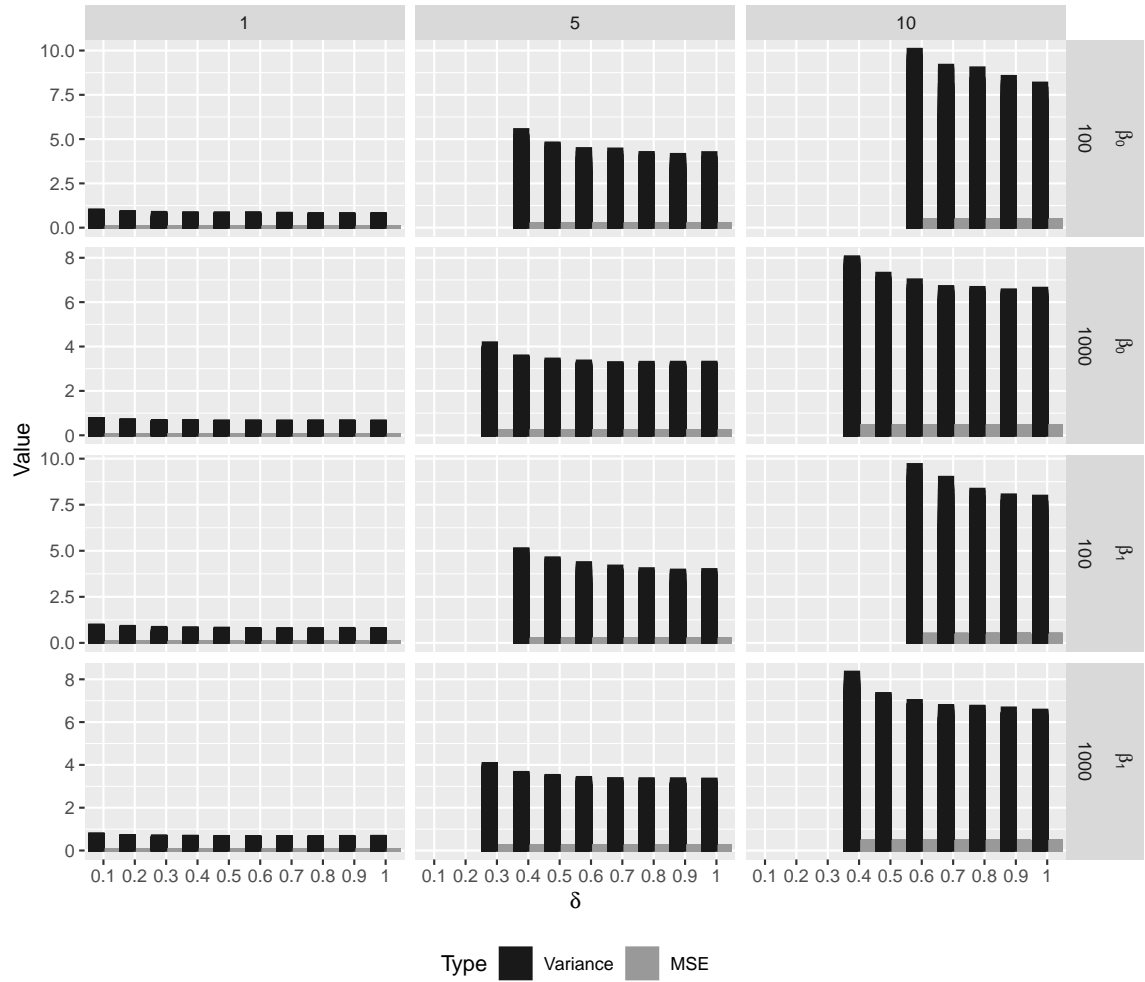


Figure 8: Mean squared error (MSE) and variance estimates of the estimated stochastic gradients. The columns represent the batch size (S) and the rows represent the sample size (n) and parameter. Smaller values indicate a better value. Estimates are given across an appropriate range of δ and averaged across 100 simulated data sets.

E Additional details on Simulation 4.2

E.1 Bernoulli Distribution

In this section, we derive the Gibbs sampler for the logistic regression with subject-specific intercept and slope. The model is given as follows, $Y_{it} \stackrel{\text{iid}}{\sim} \text{Bernoulli}(\pi_{it})$, where $\text{logit}(\pi_{it}) = \mathbf{x}_{it}^\top \boldsymbol{\beta} + \mathbf{z}_{it}^\top \boldsymbol{\gamma}_i$ and $\boldsymbol{\gamma}_i | \boldsymbol{\Sigma} \stackrel{\text{iid}}{\sim} \mathcal{N}(\mathbf{0}, \boldsymbol{\Sigma})$. We consider the scenario where $\mathbf{x}_{it} = (1, x_{it})^\top$ and $\mathbf{z}_{it} = \mathbf{x}_{it}$.

We are interested in the posterior distribution of the parameters $(\boldsymbol{\beta}, \boldsymbol{\Sigma}, \boldsymbol{\gamma}_1, \dots, \boldsymbol{\gamma}_n)$. Note that when using a standard MCMC algorithm, we require sampling of the subject specific parameters, because with logistic regression we must use the conditional model. We will augment the likelihood with a latent parameter,

$$p(Y_{it}, \omega_{it} | \boldsymbol{\beta}, \boldsymbol{\gamma}_i, \phi) = p(Y_{it} | \boldsymbol{\beta}, \boldsymbol{\gamma}_i, \phi) p(\omega_{it} | \boldsymbol{\beta}, \boldsymbol{\gamma}_i, \phi),$$

where $\omega_{it} \sim \text{PG}(1, 0)$ is a Pólya-Gamma random variable. This likelihood permits conjugacy in $\boldsymbol{\beta}$ and $\boldsymbol{\gamma}_i$ and does not alter the posterior. Polson et al. (2013) showed that $p(\omega_{it} | \boldsymbol{\beta}, \boldsymbol{\gamma}_i, \phi)$ is a tilted version of the Pólya-Gamma with the following density,

$$\begin{aligned} p(\omega_{it} | \boldsymbol{\beta}, \boldsymbol{\gamma}_i, \phi) &= \exp \left\{ -\frac{(\mathbf{x}_{it}^\top \boldsymbol{\beta} + \mathbf{z}_{it}^\top \boldsymbol{\gamma}_i)^2 \omega_{it}}{2} \right\} \cosh^{-1} \left(\frac{\mathbf{x}_{it}^\top \boldsymbol{\beta} + \mathbf{z}_{it}^\top \boldsymbol{\gamma}_i}{2} \right) f(\omega_{it}) \\ &= \exp \left\{ -\frac{(\mathbf{x}_{it}^\top \boldsymbol{\beta} + \mathbf{z}_{it}^\top \boldsymbol{\gamma}_i)^2 \omega_{it}}{2} \right\} \left(\frac{1 + \exp\{\mathbf{x}_{it}^\top \boldsymbol{\beta} + \mathbf{z}_{it}^\top \boldsymbol{\gamma}_i\}}{2 \exp\{(\mathbf{x}_{it}^\top \boldsymbol{\beta} + \mathbf{z}_{it}^\top \boldsymbol{\gamma}_i)/2\}} \right) f(\omega_{it}), \end{aligned}$$

using the fact that $\cosh\{x\} = (1 + \exp\{2x\})/(2 \exp\{x\})$. The likelihood can then be written as,

$$p(Y_{it}, \omega_{it} | \boldsymbol{\beta}, \boldsymbol{\gamma}_i, \phi) \propto \left[\frac{\exp\{Y_{it}(\mathbf{x}_{it}^\top \boldsymbol{\beta} + \mathbf{z}_{it}^\top \boldsymbol{\gamma}_i)\}}{1 + \exp\{\mathbf{x}_{it}^\top \boldsymbol{\beta} + \mathbf{z}_{it}^\top \boldsymbol{\gamma}_i\}} \right] p(\omega_{it} | \boldsymbol{\beta}, \boldsymbol{\gamma}_i, \phi)$$

$$\propto \exp \left\{ -\frac{\omega_{it}}{2} (Y_{it}^* - (\mathbf{x}_{it}^\top \boldsymbol{\beta} + \mathbf{z}_{it}^\top \boldsymbol{\gamma}_i))^2 \right\}$$

where $\chi_{it} = Y_{it} - 1/2$ and $Y_{it}^* = \frac{\chi_{it}}{\omega_{it}}$. Define, $\mathbf{Y}_i^* = (Y_{i1}^*, \dots, Y_{in_i}^*)^\top$, $\mathbf{x}_i = (\mathbf{x}_{i1}, \dots, \mathbf{x}_{in_i})^\top$, $\mathbf{z}_i = (\mathbf{z}_{i1}, \dots, \mathbf{z}_{in_i})^\top$, $\boldsymbol{\omega}_i = (\omega_{i1}, \dots, \omega_{in_i})^\top$, and $\mathbf{D}(\boldsymbol{\omega}_i)$ is an $n_i \times n_i$ diagonal matrix with $\boldsymbol{\omega}_i$ on the diagonal. The Gibbs sampler then proceeds as follows:

1. Sample $\boldsymbol{\gamma}_i$ using the following Gibbs step:

$$\begin{aligned} p(\boldsymbol{\gamma}_i | \mathbf{Y}_i, \boldsymbol{\omega}_i, \boldsymbol{\beta}, \Sigma, \boldsymbol{\gamma}_{-i}) &\propto \prod_{t=1}^{n_i} p(Y_{it}, \omega_{it} | \boldsymbol{\beta}, \boldsymbol{\gamma}_i) p(\boldsymbol{\gamma}_i | \Sigma) \\ &\propto \exp \left\{ -\frac{1}{2} \left[(\mathbf{Y}_i^* - (\mathbf{x}_i \boldsymbol{\beta} + \mathbf{z}_i \boldsymbol{\gamma}_i))^\top \mathbf{D}(\boldsymbol{\omega}_i) (\mathbf{Y}_i^* - (\mathbf{x}_i \boldsymbol{\beta} + \mathbf{z}_i \boldsymbol{\gamma}_i)) + \boldsymbol{\gamma}_i^\top \Sigma^{-1} \boldsymbol{\gamma}_i \right] \right\} \\ &\propto \exp \left\{ -\frac{1}{2} \left[\boldsymbol{\gamma}_i^\top (\mathbf{z}_i^\top \mathbf{D}(\boldsymbol{\omega}_i) \mathbf{z}_i + \Sigma^{-1}) \boldsymbol{\gamma}_i - 2\boldsymbol{\gamma}_i^\top (\mathbf{z}_i^\top \mathbf{D}(\boldsymbol{\omega}_i) (\mathbf{Y}_i^* - \mathbf{x}_i \boldsymbol{\beta})) \right] \right\} \\ &\sim \mathcal{N}(\mathbb{E}_{\boldsymbol{\gamma}_i}, \mathbb{V}_{\boldsymbol{\gamma}_i}), \end{aligned}$$

where $\mathbb{V}_{\boldsymbol{\gamma}_i} = (\mathbf{z}_i^\top \mathbf{D}(\boldsymbol{\omega}_i) \mathbf{z}_i + \Sigma^{-1})^{-1}$ and $\mathbb{E}_{\boldsymbol{\gamma}_i} = \mathbb{V}_{\boldsymbol{\gamma}_i} (\mathbf{z}_i^\top \mathbf{D}(\boldsymbol{\omega}_i) (\mathbf{Y}_i^* - \mathbf{x}_i \boldsymbol{\beta}))$.

2. Sample $\boldsymbol{\beta}$ using the following Gibbs step:

The posterior for $\boldsymbol{\beta}$ can be written as follows:

$$\begin{aligned} p(\boldsymbol{\beta} | \mathbf{Y}, \boldsymbol{\omega}, \boldsymbol{\gamma}, \Sigma) &\propto \prod_{i=1}^n \prod_{t=1}^{n_i} p(Y_{it}, \omega_{it} | \boldsymbol{\beta}, \boldsymbol{\gamma}_i) p(\boldsymbol{\beta}) \\ &\propto \exp \left\{ -\frac{1}{2} \left[\sum_{i=1}^n (\mathbf{Y}_i^* - (\mathbf{x}_i \boldsymbol{\beta} + \mathbf{z}_i \boldsymbol{\gamma}_i))^\top \mathbf{D}(\boldsymbol{\omega}_i) (\mathbf{Y}_i^* - (\mathbf{x}_i \boldsymbol{\beta} + \mathbf{z}_i \boldsymbol{\gamma}_i)) + \boldsymbol{\beta}^\top \Sigma_{\boldsymbol{\beta}}^{-1} \boldsymbol{\beta} \right] \right\} \\ &\propto \exp \left\{ -\frac{1}{2} \left[\boldsymbol{\beta}^\top \left(\sum_{i=1}^n \mathbf{x}_i^\top \mathbf{D}(\boldsymbol{\omega}_i) \mathbf{x}_i + \Sigma_{\boldsymbol{\beta}}^{-1} \right) \boldsymbol{\beta} - 2\boldsymbol{\beta}^\top \left(\sum_{i=1}^n \mathbf{x}_i^\top \mathbf{D}(\boldsymbol{\omega}_i) (\mathbf{Y}_i^* - \mathbf{z}_i \boldsymbol{\gamma}_i) \right) \right] \right\} \\ &\sim \mathcal{N}(\mathbb{E}_{\boldsymbol{\beta}}, \mathbb{V}_{\boldsymbol{\beta}}), \end{aligned}$$

where $\mathbb{V}_{\boldsymbol{\beta}} = (\sum_{i=1}^n \mathbf{x}_i^\top \mathbf{D}(\boldsymbol{\omega}_i) \mathbf{x}_i + \Sigma_{\boldsymbol{\beta}}^{-1})^{-1}$ and $\mathbb{E}_{\boldsymbol{\beta}} = \mathbb{V}_{\boldsymbol{\beta}} (\sum_{i=1}^n \mathbf{x}_i^\top \mathbf{D}(\boldsymbol{\omega}_i) (\mathbf{Y}_i^* - \mathbf{z}_i \boldsymbol{\gamma}_i))$.

3. Sample ω_{it} ($i = 1, \dots, n, t = 1, \dots, n_i$) using the following Gibbs step: The augmented parameters are updated as $p(\omega_{it} | \cdot) \sim \text{PG}(1, \mathbf{x}_{it}^\top \boldsymbol{\beta} + \mathbf{z}_{it}^\top \boldsymbol{\gamma}_i)$.

4. Sample σ_k using a Metropolis step for $k = 1, 2$:

We transform σ_k to the real line to facilitate sampling. Define a new parameter $\delta_{\sigma_k} = h(\sigma_k) = \log \sigma_k$, such that $\sigma_k = h^{-1}(\delta_{\sigma_k}) = \exp\{\delta_{\sigma_k}\}$ and $\left| \frac{\partial}{\partial \delta_{\sigma_k}} h^{-1}(\delta_{\sigma_k}) \right| \propto \exp\{\delta_{\sigma_k}\} = \sigma_k$. Now we can sample from the transformed proposal distribution, $\delta_{\sigma_k}^* \sim \mathcal{N}(\delta_{\sigma_k}, \Delta_{\sigma_k})$, where Δ_{σ_k} is a tuning parameter. Then we can obtain a proposal of σ_k , $\sigma_k^* = h^{-1}(\delta_{\sigma_k}^*)$. The Metropolis ratio can be calculated as

$$\begin{aligned} r &= \frac{p(\sigma_k^* | \mathbf{Y}, \boldsymbol{\gamma}, \boldsymbol{\beta}, \sigma_{-k}, \rho, \sigma^2)}{p(\sigma_k | \mathbf{Y}, \boldsymbol{\gamma}, \boldsymbol{\beta}, \sigma_{-k}, \rho, \sigma^2)} \\ &\propto \frac{p(\sigma_k^* | \nu) \left| \frac{\partial}{\partial \delta_{\sigma_k}} h^{-1}(\delta_{\sigma_k}^*) \right| \prod_{i=1}^n p(\boldsymbol{\gamma}_i | \boldsymbol{\Sigma}^*)}{p(\sigma_k | \nu) \left| \frac{\partial}{\partial \delta_{\sigma_k}} h^{-1}(\delta_{\sigma_k}) \right| \prod_{i=1}^n p(\boldsymbol{\gamma}_i | \boldsymbol{\Sigma})} \\ &\propto \frac{\sigma_k^* p(\sigma_k^* | \nu) \prod_{i=1}^n p(\boldsymbol{\gamma}_i | \boldsymbol{\Sigma}^*)}{\sigma_k p(\sigma_k | \nu) \prod_{i=1}^n p(\boldsymbol{\gamma}_i | \boldsymbol{\Sigma})} \\ &\propto \frac{p(\delta_{\sigma_k}^* | \nu) \prod_{i=1}^n p(\boldsymbol{\gamma}_i | \boldsymbol{\Sigma}^*)}{p(\delta_{\sigma_k} | \nu) \prod_{i=1}^n p(\boldsymbol{\gamma}_i | \boldsymbol{\Sigma})}. \end{aligned}$$

Now accept σ_k^* with probability $\min\{1, r\}$, otherwise keep σ_k .

5. Sample ρ using a Metropolis step:

We transform ρ to the real line to facilitate sampling. Define a new parameter $\delta_\rho = h(\rho) = \log \left(\frac{\rho - a_\rho}{b_\rho - \rho} \right)$, such that $\rho = h^{-1}(\delta_\rho) = (b_\rho \exp\{\delta_\rho\} + a_\rho) / (1 + \exp\{\delta_\rho\})$ and $\left| \frac{\partial}{\partial \delta_\rho} h^{-1}(\delta_\rho) \right| \propto \exp\{\delta_\rho\} / (1 + \exp\{\delta_\rho\})^2$. Now we can sample from the transformed proposal distribution, $\delta_\rho^* \sim \mathcal{N}(\delta_\rho, \Delta_\rho)$, where Δ_ρ is a tuning parameter. Then we can obtain a proposal of ρ , $\rho^* = h^{-1}(\delta_\rho^*)$. The Metropolis ratio can be calculated as

$$r = \frac{p(\rho^* | \mathbf{Y}, \boldsymbol{\gamma}, \boldsymbol{\beta}, \sigma_1, \sigma_2, \sigma^2)}{p(\rho | \mathbf{Y}, \boldsymbol{\gamma}, \boldsymbol{\beta}, \sigma_1, \sigma_2, \sigma^2)}$$

$$\begin{aligned}
& \propto \frac{p(\rho^*) \left| \frac{\partial}{\partial \delta_\rho} h^{-1}(\delta_\rho^*) \right| \prod_{i=1}^n p(\gamma_i | \Sigma^*)}{p(\rho) \left| \frac{\partial}{\partial \delta_\rho} h^{-1}(\delta_\rho) \right| \prod_{i=1}^n p(\gamma_i | \Sigma)} \\
& \propto \frac{\frac{\exp\{\delta_\rho^*\}}{(1+\exp\{\delta_\rho^*\})^2} \prod_{i=1}^n p(\gamma_i | \Sigma^*)}{\frac{\exp\{\delta_\rho\}}{(1+\exp\{\delta_\rho\})^2} \prod_{i=1}^n p(\gamma_i | \Sigma)}.
\end{aligned}$$

Now accept ρ^* with probability $\min\{1, r\}$, otherwise keep ρ .

6. Repeat steps 1-5 until convergence has been achieved and an adequate number of posterior samples have been obtained post-convergence.

E.2 Gaussian Distribution

To obtain the Gaussian regression from the exponential family specification, we defined $a(\phi) = \phi$, $b(\theta_{it}) = \theta_{it}/2$, $c(Y_{it}, \phi) = -0.5(Y_{it}^2/\phi - \log(\phi 2\pi))$, $\phi = \sigma^2$ and $\theta_{it} = \mu_{it}$, where the mean parameter is given by μ_{it} . This yields the model, $Y_{it} | \gamma_i, \Omega \stackrel{\text{ind}}{\sim} \mathcal{N}(\mathbf{x}_{it}^\top \beta + \mathbf{z}_{it}^\top \gamma_i, \sigma^2)$, where $\Omega = (\beta, \Sigma, \sigma^2)$.

The gradient of β is given in (11) of the main manuscript and for the Gaussian likelihood is specifically, $\nabla_\beta \log p(\mathbf{Y}_i, \gamma_{ir} | \Omega) = \mathbf{X}_i^\top (\mathbf{Y}_i - \mathbf{X}_i^\top \beta - \mathbf{X}_i^\top \gamma_{ir}) / \sigma^2$. The gradient for the variance parameters are given in (13). For the Gaussian GLMM dispersion parameter, σ^2 , we performed inference using the unconstrained parameter $\delta_\sigma = \log(\sigma)$, which has the following gradient,

$$\frac{\partial \log p(\mathbf{Y}_i | \gamma_{ir}, \Omega)}{\partial \delta_\sigma} = -n_i + \frac{(\mathbf{Y}_i - \mathbf{X}_i \beta - \mathbf{X}_i \gamma_{ir})^\top (\mathbf{Y}_i - \mathbf{X}_i \beta - \mathbf{X}_i \gamma_{ir})}{\sigma^2}.$$

Taken all together, we have defined the relevant gradient with respect to the unconstrained parameters of Ω and only need to define a sampling routine to obtain γ_{ir} from $\gamma_i | \mathbf{Y}_i, \beta$. In this setting, as in Section 4.1 of the main manuscript, the posterior has a closed form,

$p(\boldsymbol{\gamma}_i | \mathbf{Y}_i, \boldsymbol{\beta}) = \mathcal{N}(\mathbf{F}^{-1}\mathbf{G}, \mathbf{F}^{-1})$. The only difference is that the variance terms are being estimated. In this simulation we set $R = 100$. Details for the marginal and conditional Gibbs sampler are given in Sections E.2.1 and E.2.2 below.

The results for this simulation are presented in Figure 9 and 10 for the posterior mean and variance, respectively. Figure 10 presents posterior estimation of the variance on log scale. The results are consistent with the results from the Bernoulli simulation presented in the main manuscript. In general, all of the algorithms are faster to converge, compared to the Bernoulli simulation, which likely is attributable to the increased complexity in the Gibbs sampling for a Bernoulli random variable, both in the conditional Gibbs sampler and the sampling of $\boldsymbol{\gamma}_{ir}$ in the SGLD algorithm. Furthermore, we see the benefits of marginal inference as the sample size increases, as the marginal Gibbs sampler outperforms the conditional specification.

E.2.1 Gibbs Sampler Details (Conditional Specification)

In this section, we derive the Gibbs sampling algorithm for the linear mixed model using the conditional likelihood. As a reminder, the model is given by $\mathbf{Y}_i | \boldsymbol{\beta}, \boldsymbol{\gamma}_i, \sigma^2 \sim \mathcal{N}(\mathbf{X}_i \boldsymbol{\beta} + \mathbf{X}_i \boldsymbol{\gamma}_i, \sigma^2 \mathbf{I}_{n_i})$ and $\boldsymbol{\gamma}_i | \boldsymbol{\Sigma} \sim \mathcal{N}(\mathbf{0}_p, \boldsymbol{\Sigma})$. We place a Gaussian prior on $\boldsymbol{\beta}$, $p(\boldsymbol{\beta}) = \mathcal{N}(\mathbf{0}_p, \sigma_{\boldsymbol{\beta}}^2 \mathbf{I}_p)$, σ , σ_1 , and σ_2 all have a half-t with degree-of-freedom ν and scale s , and $\rho \sim \text{Uniform}(-1, 1)$.

The Gibbs sampler proceeds as follows:

1. Sample $\boldsymbol{\beta}$ from:

$$\begin{aligned} p(\boldsymbol{\beta} | \mathbf{Y}, \boldsymbol{\gamma}, \boldsymbol{\Sigma}, \sigma^2) &\propto p(\boldsymbol{\beta}) \prod_{i=1}^n p(\mathbf{Y}_i | \boldsymbol{\gamma}_i, \boldsymbol{\beta}, \sigma^2) \\ &\propto \exp \left\{ -\frac{1}{2} \left[\boldsymbol{\beta}^\top (\sigma_{\boldsymbol{\beta}}^2 \mathbf{I}_p)^{-1} \boldsymbol{\beta} \right. \right. \end{aligned}$$

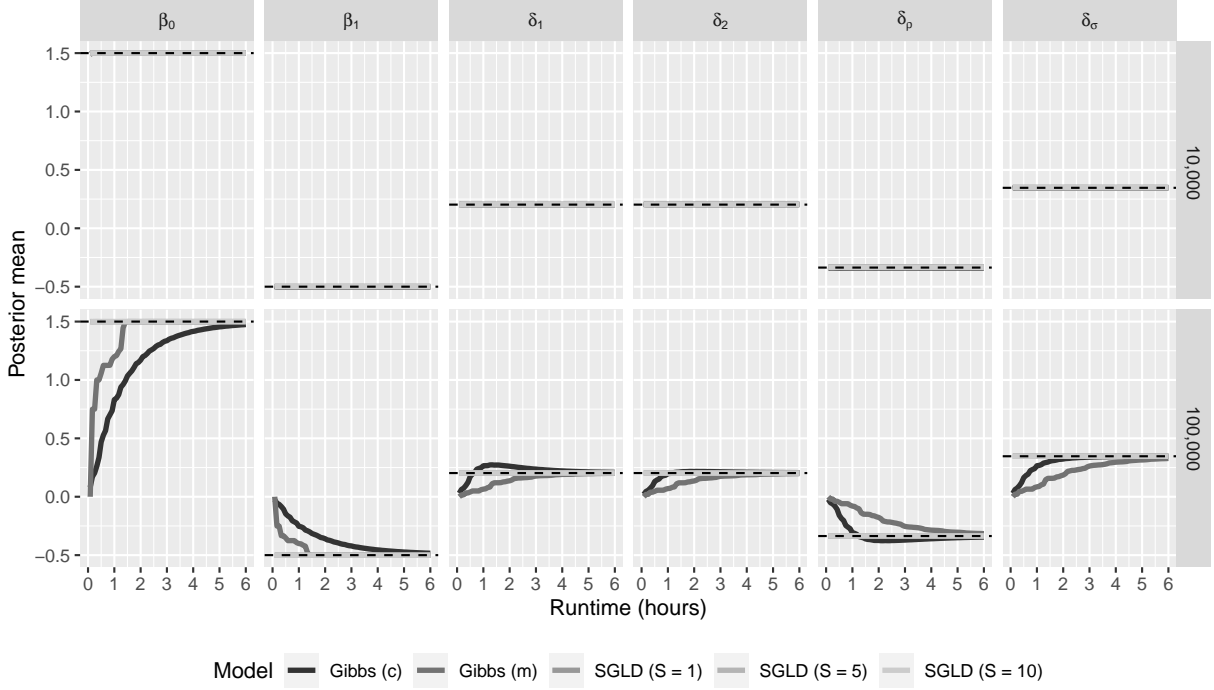


Figure 9: Posterior mean estimates presented across runtime (hours) for the linear mixed model. Columns and rows indicate parameter and sample size (n), respectively. Algorithms include Gibbs sampling, both the conditional (c) and marginal (m) specifications, and the corrected SGLD with various batch sizes (S). At each point in time, the posterior mean was calculated using the most recent 75% of the samples up to that point. Dashed black lines indicate the true value of the parameters that were used to generate the simulated data. Estimates are averaged across 100 simulated data sets.

$$\begin{aligned}
& + \sum_{i=1}^n (\mathbf{Y}_i - \mathbf{X}_i \boldsymbol{\beta} - \mathbf{X}_i \boldsymbol{\gamma}_i)^\top (\sigma^2 \mathbf{I}_{n_i})^{-1} (\mathbf{Y}_i - \mathbf{X}_i \boldsymbol{\beta} - \mathbf{X}_i \boldsymbol{\gamma}_i) \Big] \Big\} \\
& \propto \exp \left\{ -\frac{1}{2} \left[\boldsymbol{\beta}^\top \left(\frac{\mathbf{I}_p}{\sigma_{\boldsymbol{\beta}}^2} + \sum_{i=1}^n \frac{\mathbf{X}_i^\top \mathbf{X}_i}{\sigma^2} \right) \boldsymbol{\beta} - 2 \boldsymbol{\beta}^\top \left(\sum_{i=1}^n \frac{\mathbf{X}_i^\top (\mathbf{Y}_i - \mathbf{X}_i \boldsymbol{\gamma}_i)}{\sigma^2} \right) \right] \right\} \\
& \sim \mathcal{N}(\mathbb{E}_{\boldsymbol{\beta}}, \mathbb{V}_{\boldsymbol{\beta}}),
\end{aligned}$$

where $\mathbb{V}_{\boldsymbol{\beta}} = \left(\frac{\mathbf{I}_p}{\sigma_{\boldsymbol{\beta}}^2} + \sum_{i=1}^n \frac{\mathbf{X}_i^\top \mathbf{X}_i}{\sigma^2} \right)^{-1}$ and $\mathbb{E}_{\boldsymbol{\beta}} = \mathbb{V}_{\boldsymbol{\beta}} \left(\sum_{i=1}^n \frac{\mathbf{X}_i^\top (\mathbf{Y}_i - \mathbf{X}_i \boldsymbol{\gamma}_i)}{\sigma^2} \right)$.

2. Sample $\boldsymbol{\gamma}_i$ for $(i = 1, \dots, n)$ from:

$$p(\boldsymbol{\gamma}_i | \mathbf{Y}, \boldsymbol{\beta}, \boldsymbol{\Sigma}, \sigma^2) \propto p(\boldsymbol{\gamma}_i | \boldsymbol{\Sigma}) p(\mathbf{Y}_i | \boldsymbol{\gamma}_i, \boldsymbol{\beta}, \sigma^2)$$

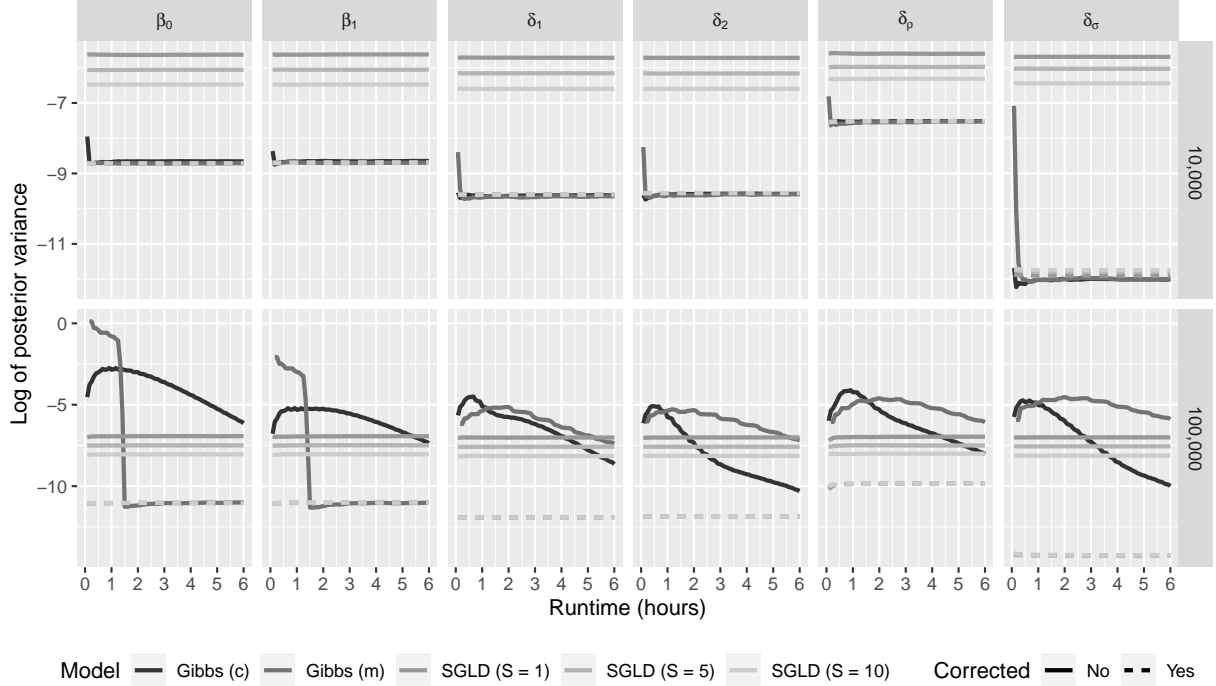


Figure 10: Log posterior variance estimates presented across runtime (hours) for the linear mixed model. Columns and rows indicate parameter and sample size (n), respectively. Algorithms include Gibbs sampling, both the conditional (c) and marginal (m) specifications, and the SGLD algorithm with various batch sizes (S). Results are presented for both the uncorrected (solid line) and corrected (dashed line) SGLD algorithm. At each point in time, the log posterior variance was calculated using the most recent 75% of the samples up to that point. Estimates are averaged across 100 simulated data sets.

$$\begin{aligned}
&\propto \exp \left\{ -\frac{1}{2} \left[\gamma_i^\top \Sigma^{-1} \gamma_i \right. \right. \\
&\quad \left. \left. + (\mathbf{Y}_i - \mathbf{X}_i \boldsymbol{\beta} - \mathbf{X}_i \boldsymbol{\gamma}_i)^\top (\sigma^2 \mathbf{I}_{n_i})^{-1} (\mathbf{Y}_i - \mathbf{X}_i \boldsymbol{\beta} - \mathbf{X}_i \boldsymbol{\gamma}_i) \right] \right\} \\
&\propto \exp \left\{ -\frac{1}{2} \left[\gamma_i^\top \left(\Sigma^{-1} + \frac{\mathbf{X}_i^\top \mathbf{X}_i}{\sigma^2} \right) \gamma_i - 2\gamma_i^\top \left(\frac{\mathbf{X}_i^\top (\mathbf{Y}_i - \mathbf{X}_i \boldsymbol{\beta})}{\sigma^2} \right) \right] \right\} \\
&\sim \mathcal{N}(\mathbb{E}_{\boldsymbol{\gamma}_i}, \mathbb{V}_{\boldsymbol{\gamma}_i}),
\end{aligned}$$

where $\mathbb{V}_{\boldsymbol{\gamma}_i} = \left(\Sigma^{-1} + \frac{\mathbf{X}_i^\top \mathbf{X}_i}{\sigma^2} \right)^{-1}$ and $\mathbb{E}_{\boldsymbol{\gamma}_i} = \mathbb{V}_{\boldsymbol{\gamma}_i} \left(\frac{\mathbf{X}_i^\top (\mathbf{Y}_i - \mathbf{X}_i \boldsymbol{\beta})}{\sigma^2} \right)$.

3. Sample σ_k using a Metropolis step for $k = 1, 2$ given in Section E.1 above.

4. Sample ρ using a Metropolis step given in Section E.1 above.

5. Sample σ using a Metropolis step:

We transform σ to the real line to facilitate sampling. Define a new parameter

$$\delta_\sigma = h(\sigma) = \log \sigma, \text{ such that } \sigma = h^{-1}(\delta_\sigma) = \exp\{\delta_\sigma\} \text{ and } \left| \frac{\partial}{\partial \delta_\sigma} h^{-1}(\delta_\sigma) \right| \propto \exp\{\delta_\sigma\} = \sigma.$$

Now we can sample from the transformed proposal distribution, $\delta_\sigma^* \sim \mathcal{N}(\delta_\sigma, \Delta_\sigma)$,

where Δ_σ is a tuning parameter. Then we can obtain a proposal of σ , $\sigma^* = h^{-1}(\delta_\sigma^*)$.

The Metropolis ratio can be calculated as

$$\begin{aligned} r &= \frac{p(\sigma^* | \mathbf{Y}, \boldsymbol{\gamma}, \boldsymbol{\beta}, \sigma_1, \sigma_2, \rho)}{p(\sigma | \mathbf{Y}, \boldsymbol{\gamma}, \boldsymbol{\beta}, \sigma_1, \sigma_2, \rho)} \\ &\propto \frac{p(\sigma^* | \nu) \left| \frac{\partial}{\partial \delta_\sigma} h^{-1}(\delta_\sigma^*) \right| \prod_{i=1}^n p(\mathbf{Y}_i | \boldsymbol{\beta}, \boldsymbol{\gamma}_i, \sigma^*)}{p(\sigma | \nu) \left| \frac{\partial}{\partial \delta_\sigma} h^{-1}(\delta_\sigma) \right| \prod_{i=1}^n p(\mathbf{Y}_i | \boldsymbol{\beta}, \boldsymbol{\gamma}_i, \sigma)} \\ &\propto \frac{p(\delta_\sigma^* | \nu) \prod_{i=1}^n p(\mathbf{Y}_i | \boldsymbol{\beta}, \boldsymbol{\gamma}_i, \sigma^*)}{p(\delta_\sigma | \nu) \prod_{i=1}^n p(\mathbf{Y}_i | \boldsymbol{\beta}, \boldsymbol{\gamma}_i, \sigma^*)}. \end{aligned}$$

Now accept σ^* with probability $\min\{1, r\}$, otherwise keep σ .

E.2.2 Gibbs Sampler Details (Marginal Specification)

In this section, we derive the Gibbs sampling algorithm for the linear mixed model using the marginal likelihood. As a reminder, the model is given by $\mathbf{Y}_i | \boldsymbol{\beta}, \boldsymbol{\Sigma}, \sigma^2 \sim \mathcal{N}(\mathbf{X}_i \boldsymbol{\beta}, \boldsymbol{\Sigma})$, where $\boldsymbol{\Sigma} = \sigma^2 \mathbf{I}_{n_i} + \mathbf{X}_i \boldsymbol{\Sigma} \mathbf{X}_i^\top$. We place a Gaussian prior on $\boldsymbol{\beta}$, $p(\boldsymbol{\beta}) = \mathcal{N}(\mathbf{0}_p, \sigma_\beta^2 \mathbf{I}_p)$, σ , σ_1 , and σ_2 all have a half-t with degree-of-freedom ν and scale s , and $\rho \sim \text{Uniform}(-1, 1)$. The Gibbs sampler proceeds as follows:

1. Sample $\boldsymbol{\beta}$ from:

$$p(\boldsymbol{\beta} | \mathbf{Y}, \boldsymbol{\Sigma}, \sigma^2) \propto p(\boldsymbol{\beta}) \prod_{i=1}^n p(\mathbf{Y}_i | \boldsymbol{\beta}, \sigma^2)$$

$$\begin{aligned}
& \propto \exp \left\{ -\frac{1}{2} \left[\boldsymbol{\beta}^\top (\sigma_{\boldsymbol{\beta}}^2 \mathbf{I}_p)^{-1} \boldsymbol{\beta} + \sum_{i=1}^n (\mathbf{Y}_i - \mathbf{X}_i \boldsymbol{\beta})^\top \boldsymbol{\Upsilon}_i^{-1} (\mathbf{Y}_i - \mathbf{X}_i \boldsymbol{\beta}) \right] \right\} \\
& \propto \exp \left\{ -\frac{1}{2} \left[\boldsymbol{\beta}^\top \left(\frac{\mathbf{I}_p}{\sigma_{\boldsymbol{\beta}}^2} + \sum_{i=1}^n \mathbf{X}_i^\top \boldsymbol{\Upsilon}_i^{-1} \mathbf{X}_i \right) \boldsymbol{\beta} - 2 \boldsymbol{\beta}^\top \left(\sum_{i=1}^n \mathbf{X}_i^\top \boldsymbol{\Upsilon}_i^{-1} \mathbf{Y}_i \right) \right] \right\} \\
& \sim \mathcal{N}(\mathbb{E}_{\boldsymbol{\beta}}, \mathbb{V}_{\boldsymbol{\beta}}),
\end{aligned}$$

where $\mathbb{V}_{\boldsymbol{\beta}} = \left(\frac{\mathbf{I}_p}{\sigma_{\boldsymbol{\beta}}^2} + \sum_{i=1}^n \mathbf{X}_i^\top \boldsymbol{\Upsilon}_i^{-1} \mathbf{X}_i \right)^{-1}$ and $\mathbb{E}_{\boldsymbol{\beta}} = \mathbb{V}_{\boldsymbol{\beta}} \left(\sum_{i=1}^n \mathbf{X}_i^\top \boldsymbol{\Upsilon}_i^{-1} \mathbf{Y}_i \right)$.

2. Sample σ_k using a Metropolis step for $k = 1, 2$:

We transform σ_k to the real line to facilitate sampling. Define a new parameter $\delta_{\sigma_k} = h(\sigma_k) = \log \sigma_k$, such that $\sigma_k = h^{-1}(\delta_{\sigma_k}) = \exp\{\delta_{\sigma_k}\}$ and $\left| \frac{\partial}{\partial \delta_{\sigma_k}} h^{-1}(\delta_{\sigma_k}) \right| \propto \exp\{\delta_{\sigma_k}\} = \sigma_k$. Now we can sample from the transformed proposal distribution, $\delta_{\sigma_k}^* \sim \mathcal{N}(\delta_{\sigma_k}, \Delta_{\sigma_k})$, where Δ_{σ_k} is a tuning parameter. Then we can obtain a proposal of σ_k , $\sigma_k^* = h^{-1}(\delta_{\sigma_k}^*)$. The Metropolis ratio can be calculated as

$$\begin{aligned}
r &= \frac{p(\sigma_k^* | \mathbf{Y}, \boldsymbol{\beta}, \sigma_{-k}, \rho, \sigma^2)}{p(\sigma_k | \mathbf{Y}, \boldsymbol{\beta}, \sigma_{-k}, \rho, \sigma^2)} \\
&\propto \frac{p(\sigma_k^* | \nu) \left| \frac{\partial}{\partial \delta_{\sigma_k}} h^{-1}(\delta_{\sigma_k}^*) \right| \prod_{i=1}^n p(\mathbf{Y}_i | \boldsymbol{\beta}, \boldsymbol{\Sigma}^*, \sigma^2)}{p(\sigma_k | \nu) \left| \frac{\partial}{\partial \delta_{\sigma_k}} h^{-1}(\delta_{\sigma_k}) \right| \prod_{i=1}^n p(\mathbf{Y}_i | \boldsymbol{\Sigma}, \sigma^2)}.
\end{aligned}$$

Now accept σ_k^* with probability $\min\{1, r\}$, otherwise keep σ_k .

3. Sample ρ using a Metropolis step:

We transform ρ to the real line to facilitate sampling. Define a new parameter $\delta_\rho = h(\rho) = \log \left(\frac{\rho - a_\rho}{b_\rho - \rho} \right)$, such that $\rho = h^{-1}(\delta_\rho) = (b_\rho \exp\{\delta_\rho\} + a_\rho) / (1 + \exp\{\delta_\rho\})$ and $\left| \frac{\partial}{\partial \delta_\rho} h^{-1}(\delta_\rho) \right| \propto \exp\{\delta_\rho\} / (1 + \exp\{\delta_\rho\})^2$. Now we can sample from the transformed proposal distribution, $\delta_\rho^* \sim N(\delta_\rho, \Delta_\rho)$, where Δ_ρ is a tuning parameter. Then we can

obtain a proposal of ρ , $\rho^* = h^{-1}(\delta_\rho^*)$. The Metropolis ratio can be calculated as

$$\begin{aligned} r &= \frac{p(\rho^* | \mathbf{Y}, \boldsymbol{\beta}, \sigma_1, \sigma_2, \sigma^2)}{p(\rho | \mathbf{Y}, \boldsymbol{\beta}, \sigma_1, \sigma_2, \sigma^2)} \\ &\propto \frac{p(\rho^*) \left| \frac{\partial}{\partial \delta_\rho} h^{-1}(\delta_\rho^*) \right| \prod_{i=1}^n p(\mathbf{Y}_i | \boldsymbol{\beta}, \boldsymbol{\Sigma}^*, \sigma^2)}{p(\rho) \left| \frac{\partial}{\partial \delta_\rho} h^{-1}(\delta_\rho) \right| \prod_{i=1}^n p(\mathbf{Y}_i | \boldsymbol{\beta}, \boldsymbol{\Sigma}, \sigma^2)}. \end{aligned}$$

Now accept ρ^* with probability $\min\{1, r\}$, otherwise keep ρ .

4. Sample σ using a Metropolis step:

We transform σ to the real line to facilitate sampling. Define a new parameter

$$\delta_\sigma = h(\sigma) = \log \sigma, \text{ such that } \sigma = h^{-1}(\delta_\sigma) = \exp\{\delta_\sigma\} \text{ and } \left| \frac{\partial}{\partial \delta_\sigma} h^{-1}(\delta_\sigma) \right| \propto \exp\{\delta_\sigma\} = \sigma.$$

Now we can sample from the transformed proposal distribution, $\delta_\sigma^* \sim \mathcal{N}(\delta_\sigma, \Delta_\sigma)$,

where Δ_σ is a tuning parameter. Then we can obtain a proposal of σ , $\sigma^* = h^{-1}(\delta_\sigma^*)$.

The Metropolis ratio can be calculated as

$$\begin{aligned} r &= \frac{p(\sigma^* | \mathbf{Y}, \boldsymbol{\beta}, \sigma_1, \sigma_2, \rho)}{p(\sigma | \mathbf{Y}, \boldsymbol{\beta}, \sigma_1, \sigma_2, \rho)} \\ &\propto \frac{p(\sigma^* | \nu) \left| \frac{\partial}{\partial \delta_\sigma} h^{-1}(\delta_\sigma^*) \right| \prod_{i=1}^n p(\mathbf{Y}_i | \boldsymbol{\beta}, \boldsymbol{\Sigma}, \sigma^*)}{p(\sigma | \nu) \left| \frac{\partial}{\partial \delta_\sigma} h^{-1}(\delta_\sigma) \right| \prod_{i=1}^n p(\mathbf{Y}_i | \boldsymbol{\beta}, \boldsymbol{\Sigma}, \sigma)}. \end{aligned}$$

Now accept σ^* with probability $\min\{1, r\}$, otherwise keep σ .

E.3 Poisson Distribution

In this simulation, we studied the performance of our algorithm in a Poisson GLMM setting, where the marginal log-likelihood cannot be found in closed form. To obtain Poisson regression from the exponential family specification, we defined $a(\phi) = 1$, $b(\theta_{it}) = \exp\{\theta_{it}\}$, $c(Y_{it}, \phi) = -\log(Y_{it}!)$, $\phi = 1$, and $\theta_{it} = \log(\lambda_{it})$. The mean parameter is given by $\mu_{it} = \lambda_{it} =$

$\exp\{\theta_{it}\}$. This yields the model, $Y_{it}|\boldsymbol{\gamma}_i, \boldsymbol{\Omega} \stackrel{\text{ind}}{\sim} \text{Poisson}(\lambda_{it})$, where $\log(\lambda_{it}) = \mathbf{x}_{it}^\top \boldsymbol{\beta} + \mathbf{z}_{it}^\top \boldsymbol{\gamma}_i$, and $\boldsymbol{\Omega} = \{\boldsymbol{\beta}, \boldsymbol{\Sigma}\}$.

The gradient of $\boldsymbol{\beta}$ is given in (11) of the main manuscript and for the Poisson likelihood is specifically, $\nabla_{\boldsymbol{\beta}} \log p(\mathbf{Y}_i, \boldsymbol{\gamma}_{ir} | \boldsymbol{\Omega}) = \mathbf{X}_i^\top (\mathbf{Y}_i - \boldsymbol{\lambda}_{ir})$, where $\boldsymbol{\lambda}_{ir} = (\lambda_{ir1}, \dots, \lambda_{irn_i})^\top$. The gradient for the variance parameters are given in (13) of the main manuscript. Taken all together, we have defined the relevant gradient with respect to the unconstrained parameters of $\boldsymbol{\Omega}$ and only need to define a sampling routine to obtain $\boldsymbol{\gamma}_{ir}$ from $\boldsymbol{\gamma}_i | \mathbf{Y}_i, \boldsymbol{\beta}$. In the setting of log Poisson regression, the subject-specific parameters do not have closed form full conditional distributions, so we used a Metropolis Hastings algorithm. Proposal values were sampled from $\boldsymbol{\gamma}_{ir}^* \sim \mathcal{N}(\boldsymbol{\gamma}_{ir}, \boldsymbol{\Delta})$, where $\boldsymbol{\Delta}$ is a tuning parameter. The Metropolis ratio was calculated as

$$r = \frac{p(\boldsymbol{\gamma}_{ir}^* | \mathbf{Y}_i, \boldsymbol{\Omega})}{p(\boldsymbol{\gamma}_{ir} | \mathbf{Y}_i, \boldsymbol{\Omega})} = \frac{p(\mathbf{Y}_i | \boldsymbol{\gamma}_{ir}^*, \boldsymbol{\beta}) p(\boldsymbol{\gamma}_{ir}^* | \boldsymbol{\Sigma})}{p(\mathbf{Y}_i | \boldsymbol{\gamma}_{ir}, \boldsymbol{\beta}) p(\boldsymbol{\gamma}_{ir} | \boldsymbol{\Sigma})},$$

and the proposal, $\boldsymbol{\gamma}_{ir}^*$, was accepted with probability $\min\{1, r\}$, otherwise we kept $\boldsymbol{\gamma}_{ir}$. The algorithm was implemented with $R = 100$ after a burn-in period where the acceptance rate was tuned to be approximately 40%. In this simulation, the true values of the variances of $\boldsymbol{\Sigma}$ were changed to 0.4 to generate more realistic Poisson random variables. Details for the conditional Gibbs sampler for Poisson regression are given in Section E.3.1 below.

The results for this simulation are presented in Figure 11 and Figure 12 of the supplementary materials for the posterior mean and variance, respectively. The conclusions are consistent with the Gaussian and Bernoulli simulations. For the Poisson results, we also presented results for a sample size of 1,000 to have a comparison with Gibbs sampling in a setting where convergence can be observed. These results confirm that the corrected SGLD algorithm is a scalable technique for inference in the GLMM setting that maintains proper uncertainty quantification.

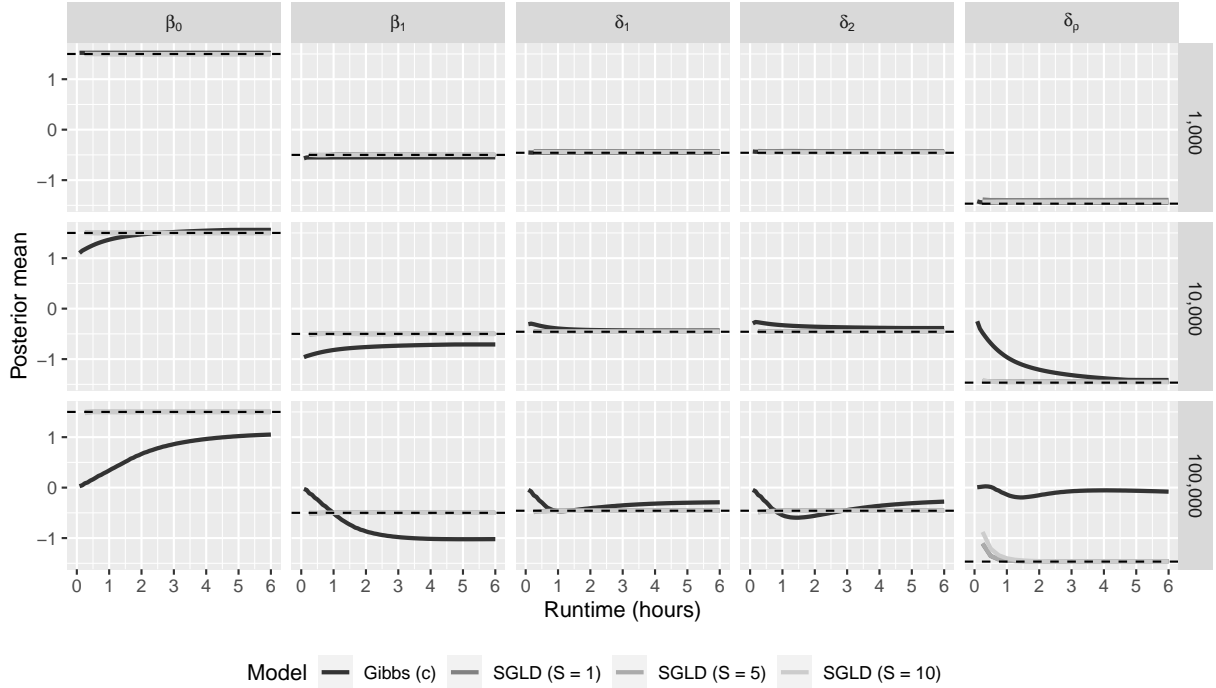


Figure 11: Posterior mean estimates presented across runtime (hours) for the Poisson mixed model. Columns and rows indicate parameter and sample size (n), respectively. Algorithms include Gibbs sampling, only the conditional (c) specification, and the corrected SGLD with various batch sizes (S). At each point in time, the posterior mean was calculated using the most recent 75% of the samples up to that point. Dashed black lines indicate the true value of the parameters that were used to generate the simulated data. Estimates are averaged across 100 simulated data sets.

E.3.1 Gibbs Sampler Details

In this section, we derive the Gibbs sampler for the Poisson regression with subject-specific intercept and slope. The model is given as follows, $Y_{it} \stackrel{\text{iid}}{\sim} \text{Poisson}(\lambda_{it})$, where $\log(\lambda_{it}) = \mathbf{x}_{it}^\top \boldsymbol{\beta} + \mathbf{z}_{it}^\top \boldsymbol{\gamma}_i$ and $\boldsymbol{\gamma}_i | \boldsymbol{\Sigma} \stackrel{\text{iid}}{\sim} \mathcal{N}(\mathbf{0}, \boldsymbol{\Sigma})$. We consider the scenario where $\mathbf{x}_{it} = (1, x_{it})^\top$ and $\mathbf{z}_{it} = \mathbf{x}_{it}$. There are no closed form full conditionals, so all updates are Metropolis steps.

1. Sample $\boldsymbol{\gamma}_i$ using the following Metropolis step:

We will sample proposal values from $\boldsymbol{\gamma}_i^* \sim \mathcal{N}(\boldsymbol{\gamma}_i, \boldsymbol{\Delta})$, where $\boldsymbol{\Delta}$ is a tuning parameter.

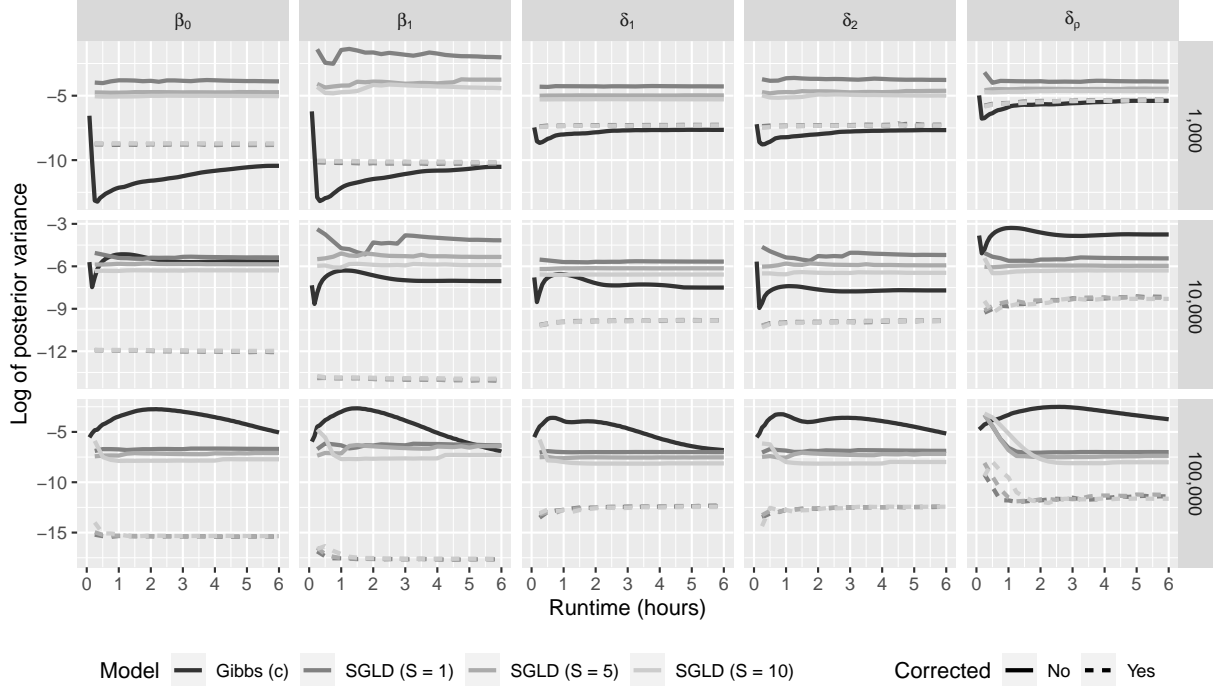


Figure 12: Log posterior variance estimates presented across runtime (hours) for the Poisson mixed model. Columns and rows indicate parameter and sample size (n), respectively. Algorithms include Gibbs sampling, only the conditional (c) specification, and the SGLD algorithm with various batch sizes (S). Results are presented for both the uncorrected (solid line) and corrected (dashed line) SGLD algorithm. At each point in time, the log posterior variance was calculated using the most recent 75% of the samples up to that point. Estimates are averaged across 100 simulated data sets.

The Metropolis ratio can be calculated as

$$\begin{aligned} r &= \frac{p(\boldsymbol{\gamma}_i^* | \mathbf{Y}_i, \boldsymbol{\Omega})}{p(\boldsymbol{\gamma}_i | \mathbf{Y}_i, \boldsymbol{\Omega})} \\ &= \frac{p(\mathbf{Y}_i | \boldsymbol{\gamma}_i^*, \boldsymbol{\beta}) p(\boldsymbol{\gamma}_i^* | \boldsymbol{\Sigma})}{p(\mathbf{Y}_i | \boldsymbol{\gamma}_i, \boldsymbol{\beta}) p(\boldsymbol{\gamma}_i | \boldsymbol{\Sigma})}. \end{aligned}$$

Now accept $\boldsymbol{\gamma}_i^*$ with probability $\min\{1, r\}$, otherwise keep $\boldsymbol{\gamma}_i$.

2. Sample $\boldsymbol{\beta}$ using the following Gibbs step:

We will sample proposal values from $\boldsymbol{\beta}^* \sim \mathcal{N}(\boldsymbol{\beta}, \boldsymbol{\Delta})$, where $\boldsymbol{\Delta}$ is a tuning parameter.

The Metropolis ratio can be calculated as

$$\begin{aligned} r &= \frac{p(\boldsymbol{\beta}^* | \mathbf{Y}, \boldsymbol{\Omega})}{p(\boldsymbol{\beta} | \mathbf{Y}, \boldsymbol{\Omega})} \\ &= \frac{p(\boldsymbol{\beta}^*) \prod_{i=1}^n p(\mathbf{Y}_i | \boldsymbol{\gamma}_i, \boldsymbol{\beta}^*)}{p(\boldsymbol{\beta}) \prod_{i=1}^n p(\mathbf{Y}_i | \boldsymbol{\gamma}_i, \boldsymbol{\beta})}. \end{aligned}$$

Now accept $\boldsymbol{\beta}^*$ with probability $\min\{1, r\}$, otherwise keep $\boldsymbol{\beta}$.

3. Sample σ_k using a Metropolis step for $k = 1, 2$ given in Section E.1 above.
4. Sample ρ using a Metropolis step given in Section E.1 above.
5. Repeat steps 1-4 until convergence has been achieved and an adequate number of posterior samples have been obtained post-convergence.

F Real Data Analysis

Table 1: Summary of patient demographics presented across an indidicator of having any distress during follow-up.

Variable	All	Distress	Other
n	40,326	6,069 (15%)	34,257 (85%)
Number of Encounters			
Mean (SD)	8.88 (9.85)	9.90 (11.15)	8.70 (9.59)
Median [Min, Max]	6 [2, 134]	6 [2, 133]	6 [2, 134]
Follow-up (Years)	3.83 (2.09)	4.15 (2.08)	3.77 (2.08)
Age (Years at baseline)	60.17 (16.69)	60.30 (15.79)	60.15 (16.84)
Gender (Male)	16,564 (41%)	1,743 (29%)	14,821 (43%)
Race			
White	27,322 (68%)	4,239 (70%)	23,083 (67%)
African American/Black	10,574 (26%)	1,573 (26%)	9,001 (26%)
Asian	1,345 (3%)	103 (2%)	1,242 (4%)
Other	1,085 (3%)	154 (3%)	931 (3%)
Insurance			
Commercial	15,013 (37%)	2,054 (34%)	12,959 (38%)
Medicaid	1,403 (3%)	341 (6%)	1,062 (3%)
Medicare	18,482 (46%)	3,103 (51%)	15,379 (45%)
Other	5,428 (13%)	571 (9%)	4,857 (14%)
Ethnicity (Hispanic/Latino)	1,161 (3%)	172 (3%)	989 (3%)
Marital Status (Single)	16,773 (42%)	3,114 (51%)	13,659 (40%)
Alcohol Use	19,813 (49%)	3,376 (56%)	16,437 (48%)
Smoking Use	16,528 (41%)	3,011 (50%)	13,517 (39%)
Illicit-Drug Use	1,276 (3%)	420 (7%)	856 (2%)
Annual Income (\$10,000)	33.02 (17.93)	32.68 (16.98)	33.08 (18.10)
Education (%)	0.87 (0.13)	0.87 (0.13)	0.87 (0.13)

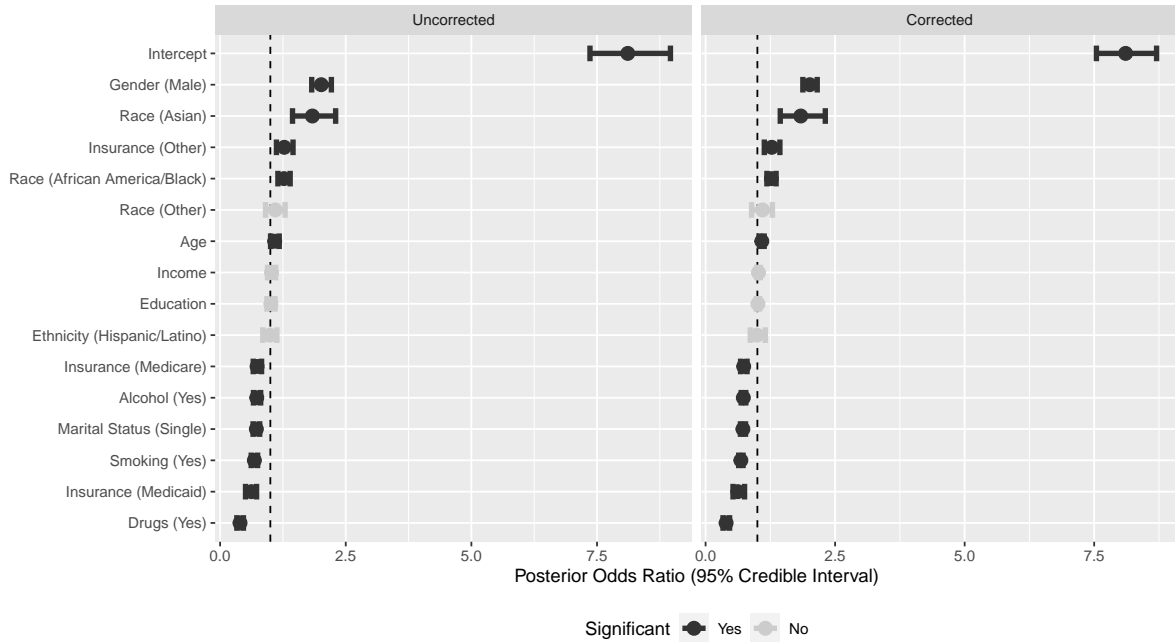


Figure 13: Posterior odds ratios and 95% credible intervals for α . Posterior summaries are presented for the uncorrected and corrected SGLD algorithm. The parameters are presented in decreasing order and color coded based on whether the credible interval contained zero.

Table 2: Posterior mean and 95% credible interval for variance parameters presented for the uncorrected and corrected SGLD algorithm.

Parameter	Corrected	Posterior Mean (95% Credible Interval)
σ_1	Yes	0.13 (0.11, 0.14)
	No	0.13 (0.11, 0.14)
σ_2	Yes	8.11 (7.54, 8.70)
	No	8.11 (7.36, 8.96)
ρ	Yes	0.04 (0.02, 0.06)
	No	0.04 (0.00, 0.08)